https://doi.org/10.5194/egusphere-2025-2641
Preprint. Discussion started: 8 July 2025

Cryosphere and ocean variability in Kane Basin since the 18th century: insights from two marine multi-proxy records

Anna Bang Kvorning[1,2], Marie-Alexandrine Sicre[3], Gregor Luetzenburg[1], Sabine Schmidt[4], Thorbjørn Joest Andersen[5], Vincent Klein[6], Eleanor Georgiadis[4,7], Audrey Limoges[8], Jacques Giraudeau[4], Anders Anker Bjørk[5], Nicolaj Krog Larsen[2] and Sofia Ribeiro[1,2]

[1]Department of Glaciology and Climate, Geological Survey of Denmark and Greenland, Copenhagen, 1350, Denmark
[2]Globe Institute, University of Copenhagen, Copenhagen, 1350, Denmark
[3]LOCEAN, CNRS, Sorbonne Université, Campus Pierre et Marie Curie, Paris, 75252, France
[4]CNRS, UMR 5805 EPOC, Université de Bordeaux, Pessac, 33615, France
[5]Department of Geosciences and Natural Resource Management, University of Copenhagen, Copenhagen, 1350, Denmark.
[6]Sorbonne University, CNRS, EPHE, UMR, 7619 METIS, Paris, 75005, France
[7]Université Laval, CNRS, UMI 3376 TAKUVIK, Québec City, QC, G1V 0A6, Canada
[8]Department of Earth Sciences, University of New Brunswick, Fredericton, NB, E3B 5A3, Canada

Correspondence to: Sofia Ribeiro (SRI@geus.dk) and Anna Bang Kvorning (asbn@geus.dk)

Abstract. Nares Strait, a marine gateway connecting the Arctic Ocean with northern Baffin Bay, is characterised by the formation of a seasonal ice bridge between Canada and Greenland, that prevents the southward export of multiyear sea ice. Recent observations indicate increasing instability in sea-ice formation particularly evident in Kane Basin, which either freezes over or remains open during winter and spring depending on ice-bridge dynamics. The Kane Basin is influenced by contrasting ocean currents in its eastern and western sides, as well as by the Humboldt Glacier, Greenland's widest marine-terminating glacier. Kane Basin is a critical region due to its pronounced sensitivity to cryospheric and oceanic changes. However, its long-term environmental history, particularly in the eastern sector, remains poorly constrained prior to the satellite era. Here, we present two multi-proxy sediment core records from opposite sides of Kane Basin, spanning from the 18th century to the present, that we compare with Humboldt Glacier frontal positions since 1965 CE. Clear spatial differences are evident across the basin in terms of sediment delivery, primary productivity, and the source of organic matter. Both records also reveal temporal changes, transitioning from cold sea-surface conditions with extensive sea ice during the Little Ice Age (LIA) (peaking around 1900 CE), towards more open and stratified waters, accompanied by increased primary production from approximately 1950 CE to the present.

https://doi.org/10.5194/egusphere-2025-2641
Preprint. Discussion started: 8 July 2025

Short summary

We compare two marine sediment cores collected from two contrasting locations in Kane Basin, northwest Greenland. The two sites differ in terms of how much sediment they receive, the level of primary biological production, and the source of organic matter. Despite these spatial differences, both records reveal a similar long-term trend, a shift from cold, heavy sea ice influenced conditions between ca. 1750–1900 CE, towards more open, fresher, and biologically productive waters beginning around 1950 CE.

1 Introduction

Global warming is driving changes in the cryosphere, including the impending disappearance of summer sea ice in the Arctic (Kim et al., 2023; Serreze and Stroeve, 2015; Stroeve et al., 2012). The Lincoln Sea, part of the Last Ice Area (Fol et al., 2025), contains old and thick multi-year sea ice and is projected to become the last refuge for perennial sea ice in the Arctic. However, accelerated loss of multi-year sea ice is now observed due to enhanced export through Nares Strait, a waterway separating Greenland from Ellesmere Island in Canada and connecting the Lincoln Sea in the Arctic Ocean to northern Baffin Bay (Moore et al., 2021).

The 530 km-long Nares Strait became an open conduit between 9000 and 8300 calibrated years before present (cal yrs BP), after the Greenland Ice Sheet and the Innuitian Ice Sheet retreated (Georgiadis et al., 2018, 2020; Jennings et al., 2011). This led to the establishment of the modern ocean circulation in Baffin Bay and the Labrador Sea (Georgiadis et al., 2018, 2020; Jennings et al., 2011). Nares Strait serves as a dual gateway with distinct oceanographic conditions on the western and eastern sides (Joli et al., 2018). On the western side, a southward-flowing current from the Arctic Ocean carries nutrient-rich Pacific water, river discharge, local precipitation, and sea-ice melt in the upper 70–110 m, underlain by warm, saline waters of Atlantic origin (Kirillov et al., 2022; Melling et al., 2001). The strait is bordered by several major marine-terminating glaciers, including Petermann Glacier and Humboldt Glacier. Humboldt Glacier, located on the eastern side of Nares Strait, is the widest outlet glacier in Greenland with a ca. 100 km-long calving front. The glacier has been retreating at an accelerated pace and is projected to contribute with 6.2–8.7 mm to global sea-level rise by 2100 under high-emission warming scenarios (Hillebrand et al., 2022). The retreat has mostly been attributed to ocean warming, leading to undercutting of the glacier (Rignot et al., 2019). Humboldt Glacier terminates in Kane Basin (Fig. 1), a 120 km-wide basin covering an area of 27,000 km^2.

A cyclonic gyre in Kane Basin slows the southward drift of sea ice and icebergs through Nares Strait (Nutt, 1966). This circulation pattern, combined with the unique shape and bathymetry of Nares Strait, facilitates the formation of ice bridges. These ice bridges typically form between late October and early April and can persist until June or July (Vincent, 2019), and they play a crucial role in regulating the export of freshwater and sea ice southward. Additionally, by blocking sea-ice movement, the bridges support the formation of the North Water (NOW) Polynya, known as Pikialasorsuaq (meaning “the

https://doi.org/10.5194/egusphere-2025-2641
Preprint. Discussion started: 8 July 2025

great upwelling") in Kalaallit Nunaat (Greenland) and Sarvarjuaq in Inuit Nunangat (Canada). This is the largest and most productive polynya in the Northern Hemisphere (Klein et al., 2002; Odate et al., 2002), supporting a diverse ecosystem including marine mammals and seabirds (Heide-Jørgensen et al., 2013).

Satellite imagery and remote sensing studies over the past three decades (1997 to present) have revealed a trend towards atypical sea-ice configurations in Nares Strait (Moore et al., 2021). Observations include a shorter duration of the ice bridges, more frequent formation of only the northern ice bridge, or even the complete absence of ice bridges (Moore et al., 2021; Vincent, 2019). The formation of ice bridges depends on factors such as cold air temperatures (below –15°C), weaker tidal forces, cessation or reversal of prevailing north-westerly winds, ice thickness, and land-fast ice stability (Kirillov et al., 2021, 2022). A decline in ice-bridge formation and stability, decreasing by 2.1 days per year between 1979 and 2019 (Vincent, 2019), has been linked to changes in ice thickness (Kirillov et al., 2021, 2022). Ice thickness, in turn, is most strongly correlated with winter wind speed in winter and spring air temperature (Ren et al., 2022). These findings are supported by marine studies indicating increased polynya instability over the same approximately 40-year period (Koerner et al., 2021, 2025; Ribeiro et al., 2021).

Kane Basin occupies a pivotal position between the typical sites of formation of the northern and southern ice bridges. When the southern ice bridge forms in Smith Sound, Kane Basin is frozen-over, whereas it remains open when only the northern bridge is present (Fig. 1d). This makes Kane Basin a crucial site for observing broader changes in the Nares Strait region. Furthermore, the basin acts as a conduit between the Last Ice Area, the sensitive NOW Polynya, and the major marine-terminating Humboldt Glacier (Fig. 1a). To capture the contrasting oceanographic conditions on both the western and eastern sides of the basin, we present two multi-proxy records, each retrieved from a strategically chosen location. These records span approximately 250 years and are integrated with 60 years of data on glacier frontal positions from historical and satellite imagery.

https://doi.org/10.5194/egusphere-2025-2641
Preprint. Discussion started: 8 July 2025

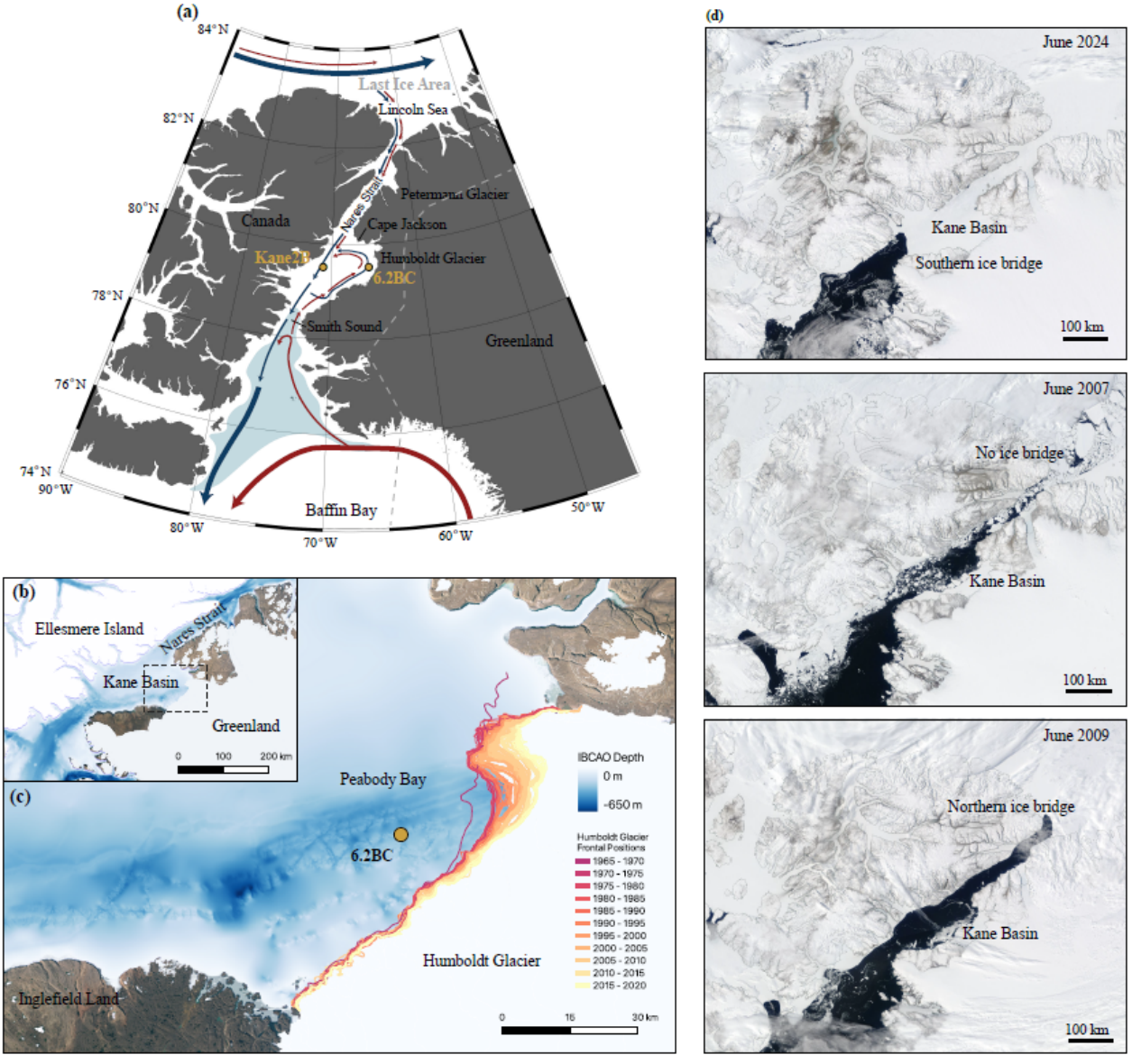

Figure 1: (a) Map illustrating the primary ocean circulation through Nares Strait, with the warm, saline West Greenland Current shown in red and the cold, fresher Baffin Current in blue. The locations of the two cores, AMD14-Kane2B-BC (Kane2B) and AMD19-6.2BC (6.2BC), are marked with yellow dots. The North Water (NOW) Polynya extent in light blue is based on (Ribeiro et al., 2021) and the Last Ice Area extent is shown by a grey dashed line based on (Fol et al., 2025). (b) Enlarged view of Kane Basin in Nares Strait, including bathymetric data obtained from the International Bathymetric Chart of the Arctic Ocean (IBCAO), Version 5 (Jakobsson et al., 2024). The dashed square indicates the location of map (c). (c) The glacier frontal positions and the centerline retreat rates for Humboldt Glacier extracted from the TermPicks Version 2 dataset (Goliber et al., 2022).

https://doi.org/10.5194/egusphere-2025-2641
Preprint. Discussion started: 8 July 2025

Terrestrial high-resolution optical satellite imagery is from the Sentinel 2 and SPOT 6/7 satellites provided by the Danish Agency for Climate Data (KDS, 2025). The data was plotted in QGIS version 3.4.3 using a polar stereographic projection centred on the North Pole (EPSG: 3413). (d) Different examples of Early-June ice bridge configuration. We acknowledge the use of imagery from NASA Worldwide application (https://worldview.earthdata.nasa.gov), part of the NASA Earth Science Data and Information System (ESDIS).

2 Methods

2.1 Sediment cores and geochronology

Box core AMD14-Kane2B-BC (hereafter Kane2B; coordinates: 79°31.140'N, 70°53.287'W; length: 32 cm; water depth: 220 m) and AMD19-6.2BC (hereafter 6.2BC; coordinates: 79°30.894'N, 65°45.252'W; length: 28 cm; water depth: 384 m) were retrieved aboard the Canadian icebreaker *CCGS Amundsen* in 2014 and 2019, respectively (Fig. 1). Sediment cores were subsampled at 1 cm resolution for Kane2B and 0.5 cm resolution for 6.2BC. The samples were weighed wet, freeze-dried and weighed again, and their volume estimated to determine the dry bulk density (DBD). Age models were developed using ^{210}Pb and ^{137}Cs measurements performed at University of Copenhagen, Denmark (6.2BC) and University of Bordeaux, France (Kane2B). Measurements were conducted with a Canberra low-background well-type Ge-detector to determine ^{210}Pb, ^{226}Ra, the difference between which was used to calculate ^{210}Pxs, and ^{137}Cs. The chronology for both records was based on mass accumulation rate (MAR) calculated from the profile of ^{210}Pbxs plotted against cumulative mass, assuming the age of the top core corresponds to the cruise year. The onset of ^{137}Cs at about 7 cm in core Kane2B and at about 12 cm in core 6.2BC validates the age-depth relationship (Fig. A1) The age-depth model was further extrapolated for determining approximate ^{210}Pb-derived ages down-core (Fig. 2). We examined each centimetre of both cores for calcareous material, such as foraminifera and shell fragments, however, neither record contained sufficient datable material to obtain reliable ^{14}C measurements.

Grain-size distribution analysis was conducted at the Geological Survey of Denmark and Greenland (GEUS), Denmark. Freeze-dried samples (ca. 2 g) were collected from Kane2B (1 cm resolution) and 6.2BC (0.5 cm resolution). These samples were wet-sieved to determine the percentage composition of clay and silt (<63 μm), fine sand (63–150 μm), and coarse sand (>150 μm).

2.2 Bulk biogeochemical analyses

Freeze-dried and homogenized samples (20–30 mg) from Kane2B (1 cm resolution) and 6.2BC (0.5–1 cm resolution) were analysed for total organic carbon (TOC), total nitrogen (TN), and the stable isotopic composition of the bulk organic matter (δ^{13}C and d^{15}N). TOC serves as an indicator of organic matter (OM) production, while stable isotope values (δ^{13}C) are used to determine the origin of OM. These values help to distinguish between different OM sources: Arctic sea ice-derived OM (–18.3‰ to –20.6‰) (Belt et al., 2008; Schubert and Calvert, 2001), marine OM (–20‰ to –22‰ in mid to low latitude regions

https://doi.org/10.5194/egusphere-2025-2641
Preprint. Discussion started: 8 July 2025

and –16.7‰ to –30.4‰ at high latitudes) (Kumar et al., 2016), and terrestrial OM (–26‰ to –28‰) (Stein and Macdonald, 2004).

The analyses were conducted at the Department of Geosciences and Natural Resource Management, University of Copenhagen, Denmark. To remove the inorganic carbon, the samples were treated with 10% hydrochloric acid (HCl) prior to analysis. Measurements were performed using an elemental analyzer coupled to either a Finnigan MAT Delta PLUS or Thermo Delta V Advantage isotope ratio mass spectrometer (Thermo Scientific, Bremen, Germany). This combined approach provides a more accurate determination of OM origin (Fig. 3) (Fernando et al., 2013; Lamb et al., 2006).

Biogenic silica (BSi) was used as an indicator of primary productivity from siliceous primary producers, mainly diatoms. Freeze-dried homogenized samples (30±1 mg) from Kane2B (1 cm resolution) and 6.2BC (0.5 cm resolution) were analysed for BSi at GEUS, Denmark, following the procedure outlined by (DeMaster, 1991). The samples were leached with 40 ml of 1% sodium carbonate (Na_2CO_3) in a warm water bath at 85°C. Subsamples (1 ml) were collected after 3, 4 and 5 hours and mixed with 9 ml of 0.021 M HCl (DeMaster, 1991). BSi concentrations were determined using the blue ammonium molybdate method on a Perkin Elmer lambda 25UV/VIS spectrophotometer (Mullin and Riley, 1955). The final BSi concentration was calculated using the average of the measurements, assuming complete dissolution of BSi after two hours of extraction (Barão et al., 2015).

2.3 Lipid biomarkers

Sea-ice reconstructions are based on the identification and quantification of source-specific highly branched isoprenoids (HBIs) and sterol biomarkers. The mono-unsaturated HBI, IP_{25} (Ice proxy with 25 carbon atoms), is produced by sea-ice dwelling diatoms of the *Haslea* and *Pleurosigma* genera (Belt, 2018; Belt et al., 2007; Belt and Müller, 2013; Brown et al., 2014). When detected in marine sediments, IP_{25} indicates seasonal sea-ice conditions. In contrast, the absence of IP_{25} in sediments suggests either permanent sea-ice cover or open water (year-round) (Belt et al., 2007; Belt and Müller, 2013). We combine IP_{25} with the tri-unsaturated HBI, HBI III, that is associated with marginal ice zone conditions(Belt et al., 2015; Kolling et al., 2020). By combining the sympagic marker with a pelagic marker such as brassicasterol or dinosterol, it becomes possible to distinguish between perennial sea ice and open water (Müller et al., 2011). The assumption behind this approach is that open-water conditions promote higher pelagic productivity, leading to elevated concentrations of these sterols.

Freeze-dried and homogenized samples (4–5 g) from Kane2B (1 cm resolution) and 6.2BC (0.5–1 cm resolution) were analysed for HBIs and sterols at LOCEAN, Sorbonne University, France, following the Standard Operating Procedure (SOP) (Belt et al., 2012). Before extraction, the internal standard 7-hexylnonadecane (7-HND) was added to each sample (10 µL). Lipid extraction was performed three times using dichloromethane (DCM) and methanol (M*e*OH) mixture (2:1, v/v). For each extraction, respectively 6, 2 and 2 ml of solvent was added to the samples, which were then ultrasonicated for 10 minutes and

https://doi.org/10.5194/egusphere-2025-2641
Preprint. Discussion started: 8 July 2025

centrifuged at 2500 rpm for 2 minutes. The resulting extracts were pooled and evaporated under a slow stream of nitrogen until dryness. The hydrocarbons, alkenones, and sterols were separated in an open silica (SiO_2) column using silica gel as a stationary phase. Elution was performed with 2.5 ml n-hexane, 4 ml n-hexane/ethyl acetate (90:10 v/v), and 4 ml n-hexane/ethyl acetate (70:30 v/v). The fractions were then evaporated under a nitrogen stream until dry. To complete derivatization, 50 µL bis-trimethylsilyl-trifluoroacetamide (BSTFA) was added to the sterol fraction and heated at 70ºC for 1 hour. The hydrocarbon, alkenone and sterol fractions were analyzed by GC-MS, gas chromatography (Agilent Technologies 7693) coupled with mass spectrometry (Agilent Technologies 5975C inert XL). The response factor for IP_{25} was determined to 9.8 for record Kane2B and 32 for record 6.2BC, calculated using four replicates of 0.1 µg and 7-HND. Compounds were identified based on their individual retention time using reference compounds and their mass spectra (Belt et al., 2007). To account for changing sedimentation rates and other sedimentary processes the biomarker concentrations were normalized to TOC (Belt and Müller, 2013).

To estimate semi-quantitative spring sea-ice conditions, we calculated the PIP index using both sympagic and pelagic markers (Müller et al., 2011) using the following Eq. (1):

$$PIP = \frac{sympagic\ marker}{sympagic\ marker + c\ \cdot pelagic\ marker}$$

where *c* represents the ratio of the mean sympagic marker to the mean pelagic marker (Müller et al., 2011). In our analysis, we used IP_{25} as the sympagic marker, while brassicasterol and dinosterol served as the pelagic markers.

2.4 Dinoflagellate cysts

Palynological processing of freeze-dried samples (ca. 2 g) from Kane2B (1 cm resolution) and 6.2BC (0.5–1 cm resolution) was conducted at Ghent University, Belgium, following the procedure described by Quaijtaal et al. (2014). One tablet of *Lycopodium* spores (batch no. 100320201), containing ca. 14,285 spores were added to each sample. The samples were treated sequentially with hydrochloric acid (2 M HCl) and hydrofluoric acid (40% HF) at room temperature to remove carbonates and dissolve siliceous material. Between acid treatments, the samples were rinsed with deionized water, sonicated, sieved through a 10 µm nylon mesh, and gently centrifuged (Quaijtaal et al., 2014). After processing, the samples were mounted on microscope slides using glycerine jelly.

Palynological analyses were performed with an Olympus BX60 transmitted light microscope at magnifications of 400x and 1000x. A minimum of 300 dinoflagellate cysts were counted per slide to ensure representative relative and absolute abundances. Furthermore, each slide was scanned for rare species. Palynomorphs, including acritarchs, pollen, copepod eggs, foraminiferal linings and *Halodinium* spp. were also counted.

https://doi.org/10.5194/egusphere-2025-2641
Preprint. Discussion started: 8 July 2025

A Principal Component Analysis (PCA) was performed on the relative abundance of dinoflagellate cysts to identify patterns in the dataset and reduce its dimensionality. The relative abundances were transformed using a Hellinger transformation (Legendre and Gallagher, 2001) and then the analysis was carried out in R (R Core Team (2021) using the vegan package (Oksanen et al., 2022). To capture basin-wide changes in Kane Basin and account for differences in the sedimentation rates of the two sites, the samples were grouped into 50-year intervals, except for the uppermost part, which covers the 14-year period from 2000 to 2014.

2.5 Generalized additive models

To detect trends across the different datasets, generalized additive models (GAMs) were applied (Hastie and Tibshirani, 1990). The analysis was conducted in R (R Core Team, 2021) using the mgcv package (Wood, 2011). GAMs are well-suited for time series with unevenly spaced data points (Simpson, 2018). The smoothing functions were parameterized using thin plate regression splines, with the number of basis functions (k) varying based on the GAMs performance. When selecting a k, we aimed to balance flexibility while preventing overfitting, with the values ranging from 3 to 8.

3 Results

3.1 Sediment cores and geochronology

The marine sediment record Kane2B was retrieved from the central Kane Basin, located farthest from the Humboldt Glacier. In both records, ^{210}Pbxs profiles present the classical exponential decrease with depth, to reach almost supported levels at about 10–15 cm (Fig. A1), suggesting a low sedimentation rate (< 0.1 cm yr^{-1}). Extrapolation of the ^{210}Pb-based chronology suggests that record Kane2B could cover approximately the last 500 years; however, given the large uncertainty associated with simple extrapolation, our focus here is on the period from ca. 1750 CE to the present. During this time, sedimentation rates ranged from 0.07 to 0.11 cm/yr, resulting in an average sample resolution of ca. 13 years (Fig. 2a). By comparison, record 6.2BC, retrieved closer to the Humboldt Glacier, covers the period from 1750 CE to the present. Sedimentation rates for this record range from 0.11 to 0.15 cm/yr, providing an average sample resolution of ca. 10 years (Fig. 2b). We note that the age-depth models are weakly constrained before 1850, as this is beyond the age limit that can suitably be dated with ^{210}Pb, and it was not possible to recover sufficient material for radiocarbon dating.

The Kane2B core varies largely in composition, with discrete samples containing 84–93% clay and silt, 7–16% fine sand, and 0–2% coarse sand (Fig. 2a). In comparison, the 6.2BC core samples are composed of 10–88% clay and silt, 1–7% fine sand, and 9–89% coarse sand (Fig. 2b). Icebergs can transport grains of all sizes, but those larger than 63µm (fine sand) are almost exclusively iceberg borne. Therefore, we define grains larger than 63µm as ice rafted debris (IRD). IRD are present in both records, but with considerably larger amounts in 6.2BC. In addition, several distinct IRD layers, defined here as intervals where grains larger than 150µm make up at least 20% of the total sediment are found at 22–22.5 cm (1762 CE), 17.5–18.5 cm

https://doi.org/10.5194/egusphere-2025-2641
Preprint. Discussion started: 8 July 2025

(1818–1812 CE), 16–17 cm (1837–1839 CE), 4.5–5.5 cm (1984–1980 CE), 3–3.5 cm (2006 CE), and 0–0.5 (2019 CE) only in record 6.2BC (Fig. 2b).

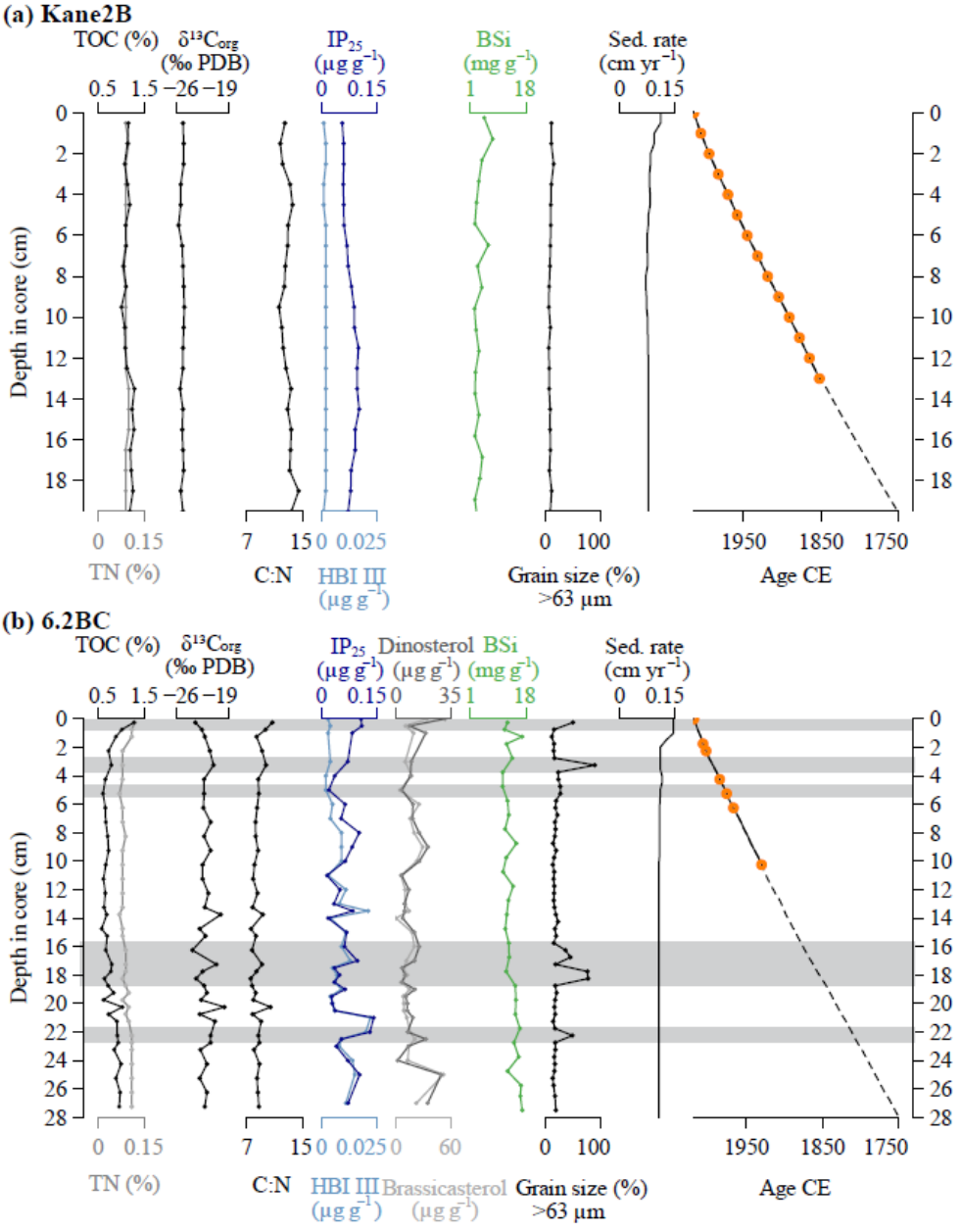

Figure 2: Marine sediment records (a) Kane2B and (b) 6.2BC. From left to right: total organic carbon (TOC) and total nitrogen (TN) weight percentages, organic carbon isotopic composition ($\delta^{13}C$), carbon-to-nitrogen ratio (C:N), concentration of lipid biomarker IP_{25} and HBI III, concentration of dinosterol and brassicasterol (exclusively for record 6.2BC (b)), biogenic silica (BSi) content, percentage of grain size >63 µm, sedimentation rate, and age-depth relationships extrapolated using sedimentation rates.

https://doi.org/10.5194/egusphere-2025-2641
Preprint. Discussion started: 8 July 2025

Actual ^{210}Pb measurements are shown as orange dots, and the dashed section of the age model indicates increased uncertainty. The grey bands highlight layers where grains larger than 150 µm constitute at least 20% of the sample.

3.2 Bulk biogeochemical analyses

The TOC content in Kane2B ranges from 1.06 to 1.29% (average 1.12%), while in 6.2BC, it ranges from 0.58 to 1.28% (average 0.79%). TN varies between 0.08 and 0.10% (average 0.09%) in Kane2B and between 0.07 and 0.12% (average 0.09%) in 6.2BC. The $\delta^{13}C$ values in Kane2B range from –25.8 to –25‰ (average –25.29‰), while in 6.2BC, $\delta^{13}C$ values range from –23.9 to –19.5‰ (average –22.05‰). Kane2B is isotopically lighter than 6.2BC, which could indicate either enhanced open-water productivity at Kane2B compared to more sea-ice-associated productivity at 6.2BC, or a higher contribution of terrestrial OM to the Kane2B site. To further evaluate this, we combined the $\delta^{13}C$ values with the C:N ratio (Meyers, 1994) (Fig. 3). In Kane2B, the C:N ratio ranges from 11.6 to 13.6 (average 12.6), while in 6.2BC, it ranges from 7.5 to 10.7 (average 8.6). In the Kane2B record, BSi concentrations ranged from 2.03 to 7.50 mg g^{-1} dry mass (average 3.44 mg g^{-1}) (Fig. 2a), while in the 6.2BC record, they range from 10.84–16.86 mg g^{-1} dry mass (mean 13.45 mg g^{-1}) (Fig. 2b).

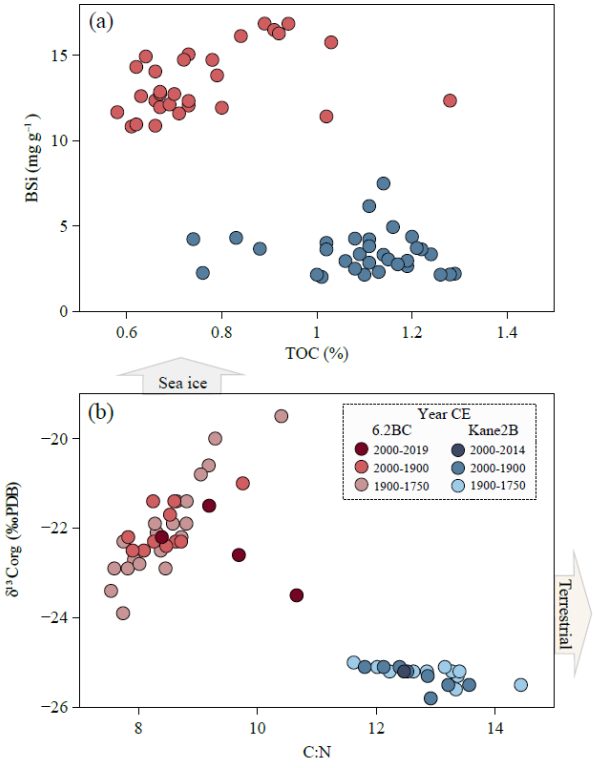

Figure 3: (a) Biogenic silica (BSi) plotted against total organic carbon (TOC) (b) Origin of the organic matter is described by plotting $\delta^{13}C$ against C:N ratio (Meyers, 1994). The blue dots show data from AMD14-Kane2B-BC and the red dots show data from AMD19-6.2BC.

https://doi.org/10.5194/egusphere-2025-2641
Preprint. Discussion started: 8 July 2025

3.3 Lipid biomarkers

In the Kane2B record, the IP_{25} concentrations vary between 0.06 and 0.10 µg g^{-1} (average 0.08 µg g^{-1}), and in the 6.2BC core between 0.02 and 0.14 µg g^{-1} (average 0.06 µg g^{-1}). When normalized to TOC, the IP_{25} concentrations in Kane2B range from 4.83 to 9.18 µg g^{-1} TOC (average 6.77 µg g^{-1} TOC), while in the 6.2BC record, the concentrations range from 2.45 to 15.47 µg g^{-1} TOC (average 8.00 µg g^{-1} TOC). In the Kane2B record, the HBI III concentrations vary between 0.001 and 0.002 µg g^{-1} (average 0.002 µg g^{-1}), and between 0.002 and 0.022 µg g^{-1} (average 0.008 µg g^{-1}) in 6.2BC. When normalized to TOC the HBI III concentrations in record Kane2B range from 0.086 to 0.203 µg g^{-1} TOC (average 0.155 µg g^{-1} TOC), while in 6.2BC, concentrations range from 0.230 to 2.986 µg g^{-1} TOC (average 1.064 µg g^{-1} TOC). Analyses of the pelagic markers brassicasterol and dinosterol were only conducted for record 6.2BC. The concentration of brassicasterol varies between 0 and 0.051 µg g^{-1} (average 0.015 µg g^{-1}) and between 0.001 and 0.031 µg g^{-1} (average 0.011 µg g^{-1}) for the dinosterol. When normalized to TOC the brassicasterol varies between 0 and 5.7 µg g^{-1} TOC (average 1.9 µg g^{-1} TOC) and the dinosterol between 0.11 and 3.18 µg g^{-1} TOC (average 1.36 µg g^{-1} TOC).

3.4 Dinoflagellate cysts

Dinoflagellate cysts are a useful proxy for sea-surface conditions. In the Kane2B record, dinoflagellate cyst concentrations range from 2851 to 5879 cysts g^{-1} (average 4236 cyst g^{-1}), while in the 6.2BC record, concentrations range from 1434 to 6699 cysts g^{-1} (average 2996 cyst g^{-1}) (Fig. A2). A total of 13 and 12 different dinoflagellate cyst taxa were identified in Kane2B and 6.2BC, respectively (Fig. A4 and A5). The assemblages in both records are dominated by heterotrophic dinoflagellate cysts, accounting for at least 94% of the total assemblage in record Kane2B and 93% in record 6.2BC. The most abundant species in both records are *Brigantedinium* spp., *Islandinium minutum* subsp. *minutum*, *Echinidinium karaense* and *Islandinium*? *cezare/cyst of Protoperidinium tricingulatim*. Notably, there is an increase in autotrophic/mixotrophic species in both records, leading up to the present day. Additionally, *Spiniferites ramosus* was only detected in Kane2B. The PCA performed on the relative abundance of dinoflagellate cysts in both records shows that axis 1 explains approximately 71% of the data variance (eigenvalue of 0.02), while axis 2 accounts for around 13% (eigenvalue of 0.003) (Fig. 4).

The PCA results reveal that the samples from 1950–2000 and 2000–2014 cluster together with most autotrophic/mixotrophic species, such as *Operculodinium centrocarpum, Pentapharsodinium dalei*, *Biecheleria* spp. and *Spiniferites elongatus*. Cysts of *Pentapharsodinium dalei* and *Biecheleria* spp. are associated with high stratification and increased freshwater input. Notably, this marks the first recorded occurrence of *Biecheleria* spp. in central Kane Basin over the past 9000 cal years BP (Caron et al., 2019). *Spiniferites elongatus* is closely associated with the sample interval 2000–2014. This species thrives in eutrophic settings, such as the North Atlantic frontal system, indicating that enhanced water stratification in Kane Basin during this period may have facilitated its increased abundance. The heterotrophic taxon *Brigantedinium* spp. also clusters with these samples, suggesting a rise in productivity from 1950 CE to the present. The presence of cyst of *P. glacialis* could reflect

https://doi.org/10.5194/egusphere-2025-2641
Preprint. Discussion started: 8 July 2025

250 improved preservation or an increase in sea-ice productivity (i.e. a longer open-water season). This statistically supported grouping highlights a shift in sea-surface conditions beginning around 1950 CE.

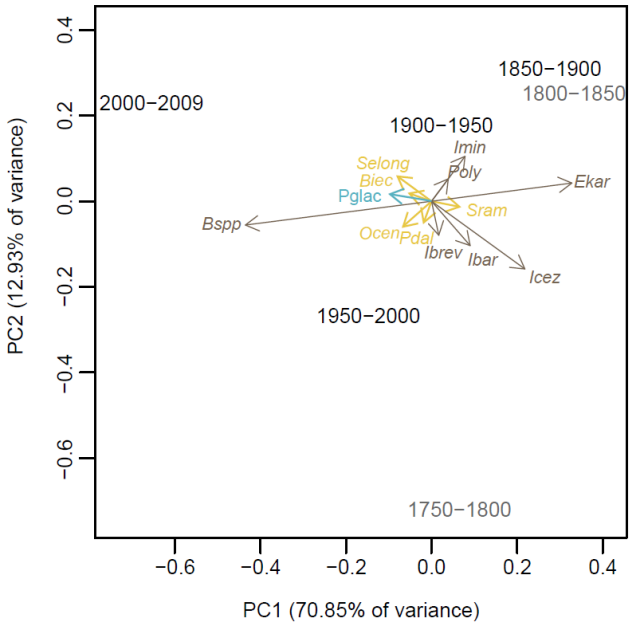

Figure 4: Principal Component Analysis (PCA) of the dinoflagellate cyst assemblage data for both records grouped into 50-year intervals. The intervals <1850 CE are plotted in grey to reflect the lower confidence in age estimation for the deeper parts of the cores. *Brigantedinium* spp. (Bspp), *Operculodinium centrocarpum* (Ocen), cyst of *Pentapharsodinium dalei* (Pdal), *Islandinium brevispinosum* (Ibrev), *Islandinium minutum* subsp. *barbatum* (Ibar), *Islandinium*? *cezare* (Icez), *Spiniferites ramosus* var. *ramosus* (Sram), *Echinidinium karaense* (Ekar), *Islandinium minutum* subsp. *minutum* (Imin), cyst of *Polykrikos*? sp. of Kunz-Pirrung (1998) – Arctic morphotype (Poly), *Spiniferites elongatus* (Selong), cyst of *Biecheleria* spp. (Biec), *Pentapharsodinium dalei* (Pdai).

4 Discussion

4.1 Spatial differences between the sites

255 The two marine sediment records collected in Kane Basin reveal significant spatial differences. The Kane2B record, retrieved from the central part of Kane Basin at 220 m water-depth, has a lower sedimentation rate, resulting in a coarser resolution with an average sample coverage of 13 years. The 6.2BC record, collected at 384 m water-depth from the eastern side of the basin and in close proximity to the Humboldt Glacier has a higher sedimentation rate, resulting in an average sample resolution of 10 years. Furthermore, the 6.2BC record contains multiple layers of IRD, where at least 20% of the total sample consists of
260 grains larger than 150µm, indicating periods of heavy iceberg activity (Fig. 2b). In contrast, such IRD layers are absent from the Kane2B record.

https://doi.org/10.5194/egusphere-2025-2641
Preprint. Discussion started: 8 July 2025

A clear spatial difference in primary production indicators is also observed between the two sites (Fig. 3a). The TOC ranges from 0.58 to 1.29% in both records. A study of surface sediments from Petermann Fjord, Hall Basin, northern Kennedy Channel, and southern Robeson Channel reports TOC values between 0.09 and 0.23%, with the highest values linked to sites with increased mobile sea ice (Jennings et al., 2020). Thus, the elevated TOC values in Kane Basin may indicate more mobile sea ice compared to sites further north of Kane basin. When comparing the records, core Kane2B shows generally higher TOC values compared to record 6.2BC. To further investigate the origin of TOC, a plot of $\delta^{13}C$ values against the C:N ratio provides additional insights into the composition and source of the organic material (Fig. 3b). We observe a clear difference in the OM signatures between the two sites. The average $\delta^{13}C$ value in Kane2B is –25.29‰, whereas in 6.2BC it is –22.05‰, indicating that both sites primarily receive marine OM, which typically ranges from –16.7‰ to –30.4‰ (Kumar et al., 2016). The heavier isotopic signal in 6.2BC may be explained by a greater contribution of autochthonous OM produced within sea ice (–18.3‰ to –20.6‰) (Belt et al., 2008; Schubert and Calvert, 2001), whereas the lighter isotopic signal in Kane2B suggests more contribution of terrestrial OM. This interpretation is corroborated by the C:N ratio: Kane2B has an average C:N of 12.55 that is higher than the C:N ratio for 6.2BC at 8.6. Studies have documented the presence of Siberian shelf waters in Kennedy Channel, north of Kane Basin (Burgers et al., 2023) which carry a strong dissolved terrigenous OM signal derived from Siberian river runoff (Burgers et al., 2023; Williford et al., 2022). Furthermore, the presence of micro charcoal fragments in Kane2B's dinoflagellate cyst slides (Fig. 5) is a strong indication that the site is influenced by the coal-bearing Paleogene sequences along the western coast of Nares Strait (e.g., Miall, 1982). This observation was also made in the longer gravity core Kane2B, which was retrieved from the same site (Georgiadis et al., 2018).

https://doi.org/10.5194/egusphere-2025-2641
Preprint. Discussion started: 8 July 2025

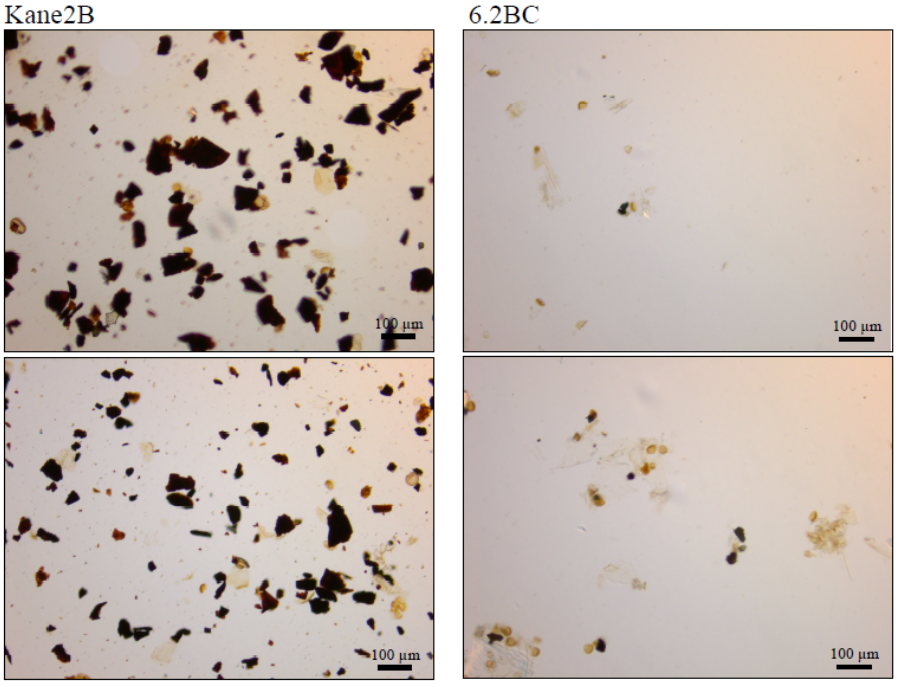

Figure 5: Visual comparison of micro charcoal fragments abundance between the two sites. Slides from Kane2B (left site) show a consistently high concentration of coal fragments throughout the record, in contrast to rare occurrences in record 6.2BC (right site).

Biogenic silica concentrations are higher in record 6.2BC compared to Kane2B, which contrasts with the pattern observed for TOC. This difference could reflect several processes. (1) Hydrodynamic conditions: diatom settling on the seafloor may be disrupted by strong wind and ocean currents flowing through the main channel of Nares Strait (Moore et al., 2021), resulting in their southward export. The more sheltered location of 6.2BC is less affected by these currents, allowing a higher proportion of diatoms to settle. (2) Nutrient availability: The eastern sector of the basin is under a greater influence of glacial meltwater, which may contribute to enhanced nutrient availability. Studies have shown that pro-glacial upwelling can increase nutrient supply, thereby fuelling primary production (Meire et al., 2017). It is possible that this mechanism also occurs near Humboldt Glacier, where meltwater is likely charged in nutrients from glacial erosion, and the upwelling of this freshwater potentially entrails nutrient-rich bottom water. It should also be considered that if such a mechanism is present, the upwelled water may include nutrient-rich Baffin Bay water originating from the polynya, which is transported northward. Furthermore, recent observations indicate the presence of a polynya near Cape Jackson in the northern Kane Basin (Fig. 1a) (Kirillov et al., 2022), which may also contribute nutrient-rich waters to the region. (3) Oceanographic differences: the observed variation may also stem from differences in ocean current influences. In Kane Basin, ocean cyclonic circulation is characterised by a southward flow along the western coast, originating from the Lincoln Sea. This flow comprises Pacific Water in the upper 100–150 m, underlain by a warmer layer associated with Atlantic Water entering through the Arctic Ocean. On the eastern side, relatively

https://doi.org/10.5194/egusphere-2025-2641
Preprint. Discussion started: 8 July 2025

warm Atlantic Water flows northward from Baffin Bay (Fig. 1a). One branch of this flow recirculates and merges with the southward-flowing current, while the other continues northward. Additionally, a cyclonic gyre in Peabody Bay influences local circulation patterns (Fig. 1c) (Kirillov et al., 2022). The eastern side of Kane Basin is therefore more influenced by Atlantic water, which is typically associated with higher nutrient availability, likely stimulating primary productivity at site 6.2BC. (4) Biological differences: it is also important to consider both the size and degree of silicification of phytoplankton species, as these factors influence the amount of biogenic silica preserved in the sediments. Additionally, differences in phytoplanktonic assemblages between the two sites may play a role. One site may be dominated by siliceous phytoplankton, such as diatoms, while the other may have a higher proportion of non-siliceous taxa, resulting in lower silica deposition.

South of Kane Basin in Baffin Bay, a spatial contrast was observed in the dinoflagellate cyst records. The eastern side exhibited both higher overall concentrations and a larger proportion of autotrophic/mixotrophic species compared to the western side (Koerner et al., 2025). This pattern was attributed to the influence of Atlantic–derived waters, supported by the high abundance of *Operculodinium centrocarpum* (e.g., de Vernal et al., 2020). While our record may reflect a similar trend of enhanced primary productivity in the eastern side, we do not observe a comparable high abundance of *Operculodinium centrocarpum* or a pronounced difference in total dinoflagellate cyst concentrations between the sites.

4.2 Glacier dynamics and ice-rafted debris

In the marine sediment record 6.2BC, located near Humboldt Glacier, multiple IRD layers were identified based on grain size analyses. The three most recent layers correspond to the periods 1976–1980±7.6 years, 1994±4.8 years, and 2017±0.4 years CE, enabling a direct comparison between IRD deposition, historical glacier front positions (Goliber et al., 2022) and solid iceberg discharge (Mouginot et al., 2019) (Fig. 6). The position of the Humboldt Glacier front has been systematically mapped from aerial photos and historical and modern satellite images since 1965 CE (Goliber et al., 2022). This was done by manually tracing the ice-ocean boundary. The Humboldt Glacier is a vast and wide outlet glacier, with two distinct zones exhibiting different calving margin behaviours. The southern zone lies on a relatively high elevation bed and is characterized by low flow speeds and minimal variability throughout the 20th century. In contrast, the most northern sector is situated over a deep subglacial trough, where flow velocities and retreat rates are high and have accelerated over the study period. In 1970 CE, the glacier experienced a significant retreat, coinciding with an IRD layer dated to 1976–1980±7.6 years. From that point onward, the glacier has continued to accelerate its retreat, accompanied by an increased sedimentation rate (Fig. 2b) and the deposition of two additional IRD layers (Fig. 6). The deposition of these two most recent IRD layers aligns with peak iceberg discharge values observed during this period (Fig. 6). These findings support the link between the observed IRD in core 6.2BC and increased iceberg production and ice marginal retreat.

https://doi.org/10.5194/egusphere-2025-2641
Preprint. Discussion started: 8 July 2025

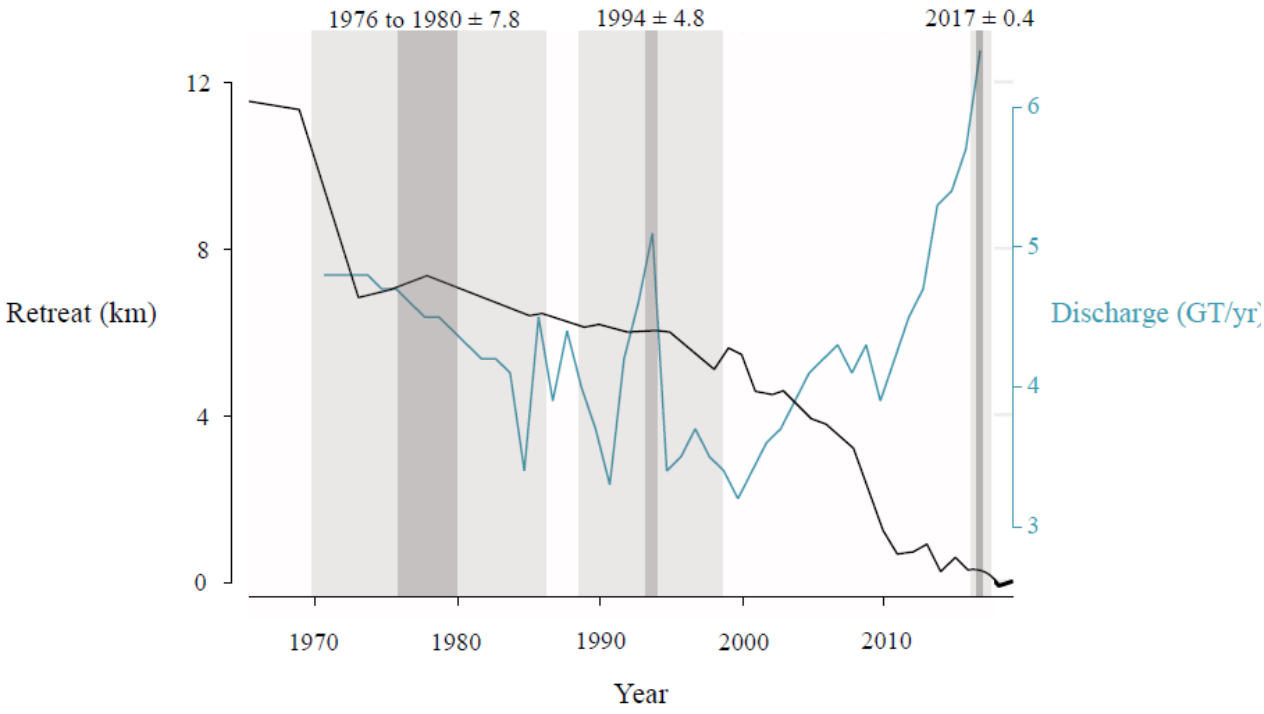

Figure 6. Estimated retreat of the Humboldt glacier since 1965 and solid ice discharge (Mouginot et al., 2019), compared with IRD layers found in the 6.2BC sediment core. The centerline retreat of Humboldt Glacier has been calculated in kilometres based on the systematically mapped front positions from 1965 CE (Goliber et al., 2022). For years with multiple frontal observations, we calculated the annual mean change rate. The dark grey bands highlight layers where grains larger than 150µm constitute at least 20% of the sample, with the age error shown in light grey.

4.3 Temporal trends in sea-ice conditions and primary productivity

In the Kane2B record, elevated concentrations of sea-ice biomarkers IP_{25} and HBI III, alongside high abundances of *Islandinium minutum* subsp. *minutum*, are observed between approximately 1750 and 1900 CE, reaching a peak around 1900 CE. *Islandinium minutum* is found in cold environments and can tolerate sea ice (e.g., Head et al., 2001). These cold conditions reconstructed in our record coincide with the LIA (Kjær et al., 2022). This period experienced the last maximum ice-sheet advance at 1900 CE, which is likely associated with factors such as lower air temperatures and ocean surface cooling(Kjær et al., 2022). Our findings further support the notion that temperatures were colder and sea-ice cover more extensive, reaching a peak around 1900 CE. GAMs indicate a declining trend from 1900 CE to the present, however, the model does not account for the high abundance of *Islandinium minutum* subsp. *minutum* in the uppermost sample, where its relative abundance exceeds 70%, a level comparable to peak LIA conditions. This finding strongly indicates cold sea-surface conditions today, possibly driven by enhanced meltwater input (Fig. 7). The dinoflagellate cyst *Polarella glacialis* appears around 1990 and persists until

https://doi.org/10.5194/egusphere-2025-2641
Preprint. Discussion started: 8 July 2025

present. The dinoflagellate cyst *Polarella glacialis* is considered a sea-ice indicator and is commonly detected in first-year sea ice and is deposited on the seabed following sea-ice melt (e.g., Harðardóttir et al., 2024; Stoecker et al., 2000). An increase in *Polarella glacialis* was also observed in the records from northern Baffin Bay starting around 1970 CE (Koerner et al., 2025). The presence of the cysts indicates improved preservation and/or an increase in first-year sea ice relative to multi-year ice.

In core 6.2BC, the concentrations of IP_{25}, HBI III, and *Islandinium minutum* subsp. *minutum* exhibit notable fluctuations. However, GAMs indicate an overall decreasing trend in HBI III and *Islandinium minutum* subsp. *minutum* toward the present day, a pattern supported by the PIP_{25} index. The PIP_{25} index was calculated for record 6.2BC, as this core was analysed for the pelagic markers brassicasterol and dinosterol (Fig. 7). The $PIP_{25,}$ which is used to assess shifts in sea-ice conditions (Müller et al., 2011), shows a transition around 1900 CE from extensive and fluctuating sea-ice cover to a more variable sea-ice cover (Fig. 7) (Müller et al., 2011). Additionally, cysts of the dinoflagellate *Polarella glacialis* appear in the record from approximately 1910 CE to the present. Combined, the findings suggest a shift from a more semi-permanent ice cover to a more seasonal and less extensive sea-ice cover, occurring earlier in the eastern part of Kane Basin than in the central region.

https://doi.org/10.5194/egusphere-2025-2641
Preprint. Discussion started: 8 July 2025

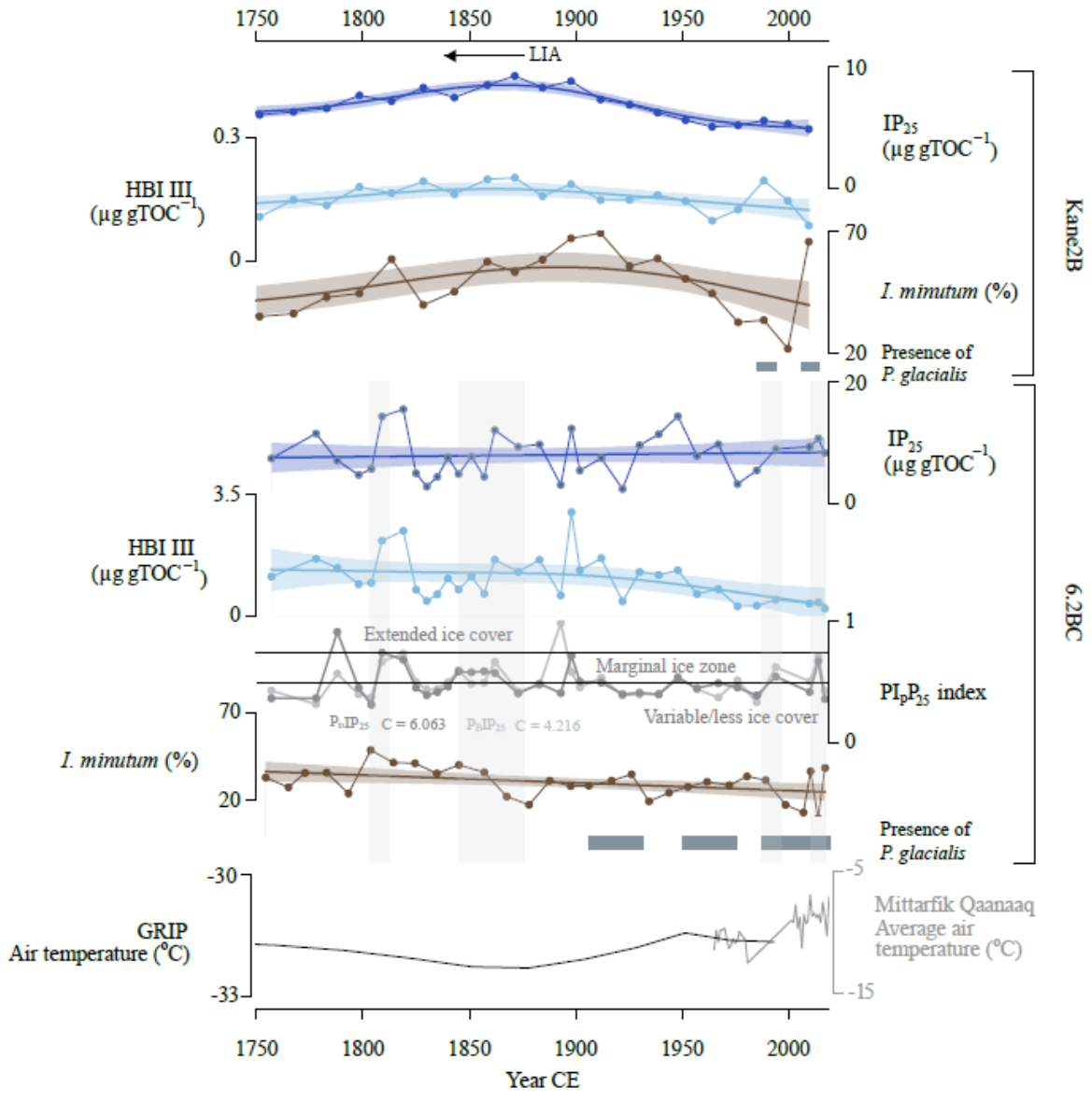

Figure 7: Inferred sea-ice conditions for the Kane2B record (top) and 6.2BC record (bottom) based on IP_{25}, HBI III, the abundances of the dinoflagellate cyst *Islandinium minutum*, and the presence or absence of *Polarella glacialis* cysts. For the 6.2BC record, the PIP_{25} index is calculated using the pelagic markers brassicasterol and dinosterol. The bottom panel displays air temperature data from the GRIP ice core record in black (Dahl-Jensen et al., 1998) and the Mittarfik Qaanaaq weather station in grey (data from the Danish Meteorological Institute (dmi.dk)). Grey bands highlight layers where grains larger than 150µm constitute at least 20% of the sample. The Little Ice Age (LIA) period is indicated by an arrow.

https://doi.org/10.5194/egusphere-2025-2641
Preprint. Discussion started: 8 July 2025

Primary productivity reconstructions are based on biogenic silica (BSi), dinoflagellate cyst concentrations, the abundance of autotrophic/mixotrophic species (and indicative of improved light availability) and TOC, which we have demonstrated to be mainly of marine origin. For record 6.2BC we also include the pelagic biomarkers brassicasterol and dinosterol (Fig. 8). To further evaluate the composition and structure of the phytoplankton community, the dinoflagellate cyst assemblage is represented as pie charts, displaying the average abundances for the periods 1750-1900 CE and 1900 CE to the present (Fig. 8).

In the Kane2B record, BSi shows a general increasing trend toward present, while the dinoflagellate cyst concentrations exhibit the opposite trend. The rising BSi values could be attributed to (1) weaker currents, resulting in reduced southward export, (2) increased BSi production in the Arctic Ocean leading to higher concentrations transported by southward-flowing currents, or (3) a shift in the primary producer composition around 1900 CE, indicating an environmental transition from conditions favouring dinoflagellate to those more supportive of diatom productivity. Furthermore, an examination of the cyst assemblage reveals a slight increase in both *Brigantedinium* spp. and autotrophic/mixotrophic species, suggesting enhanced primary productivity and light availability, respectively.

In core 6.2BC, the GAMs reveal a decreasing trend in BSi toward present; however, the model does not capture the high values from around 2000 CE until present. The dinoflagellate cyst concentrations and TOC both show a decline until approximately 1900 CE, followed by an increase toward the present. The dinosterol and brassicasterol exhibit the same trend, a slight decrease until around 1850 CE, after which they show a small rise toward the present. Furthermore, an examination of the cyst assemblage reveals an increase in both *Brigantedinium* spp. and autotrophic/mixotrophic species, like what was observed for the Kane2B record. However, the increase in *Brigantedinium* spp. abundance is more pronounced in 6.2BC. Enhanced productivity and a shift toward autotrophic/mixotrophic species relative to heterotrophic ones has also been observed in northern Baffin Bay (Koerner et al., 2025). Like our records, the authors found an increase in cysts of *Pentapharsodinium dalei*, a species associated with enhanced stratification (Heikkilä et al., 2014). These changes are attributed to increased influence of Atlantic-sourced waters and/or earlier open-water conditions.

https://doi.org/10.5194/egusphere-2025-2641
Preprint. Discussion started: 8 July 2025

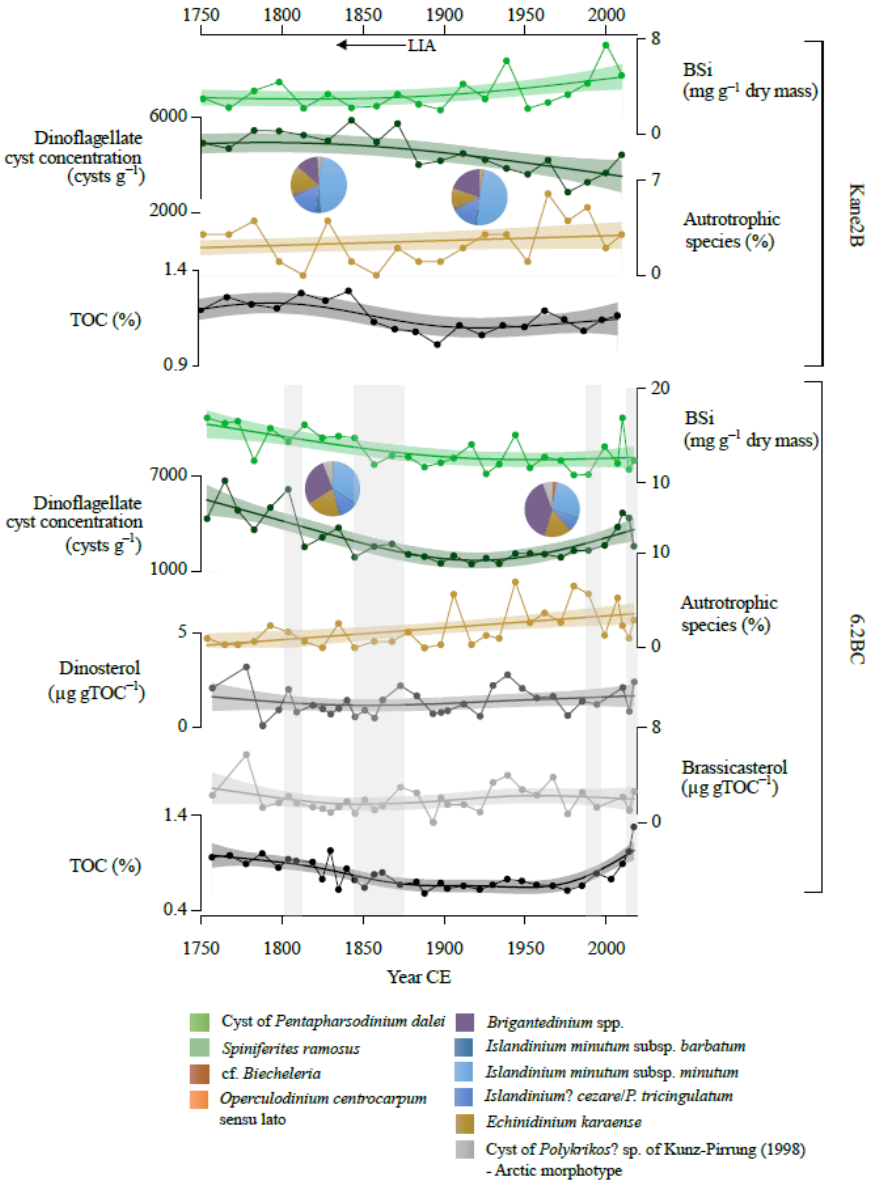

Figure 8: Primary production panel for the Kane2B record (top) and 6.2BC record (bottom) based on biogenic silica (BSi), dinoflagellate cyst concentrations, and the abundance of autotrophic/mixotrophic species. For the 6.2BC record, additional data include the pelagic biomarkers brassicasterol and dinosterol, as well as total organic carbon (TOC). Dinoflagellate cyst assemblages are represented as pie charts, showing the average abundances for the periods 1750–1900 CE and 1900 CE to the present. Grey bands highlight layers where grains larger than 150µm constitute at least 20% of the sample. The Little Ice Age (LIA) extent is indicated by an arrow.

https://doi.org/10.5194/egusphere-2025-2641
Preprint. Discussion started: 8 July 2025

4.4 Indicator region for a future Nares Strait

Our records show a clear shift around 1950 CE, marked by increased primary production and a change in the dinoflagellate cyst assemblage composition toward more autotrophic/mixotrophic species. Furthermore, we observe a rise in taxa indicative of enhanced stratification and increased freshwater input. We attribute these changes to (1) intensified freshwater runoff from the Humboldt Glacier and/or (2) a higher frequency of failed ice bridge formation, facilitating a greater freshwater export through Nares Strait, contributing to surface freshening. Observational data from the past three decades (1997–present) reveal an atypical ice configuration in Nares Strait (Moore et al., 2021), including shorter ice bridge duration, more frequent formation of only the northern ice bridge, or even the complete absence of an ice bridge (Moore et al., 2021; Vincent, 2019). An increasing trend toward the exclusive northern ice bridge limits the export of drift ice through Nares Strait, leading to more open-water conditions in Kane Basin. A previous study suggests that the persistence of the northern ice bridge therefore promotes elevated primary productivity in the region (Georgiadis et al., 2020). Based on this, we interpret the observed rise in primary production and changes in dinoflagellate cyst assemblages as a response to more frequent open-water conditions in Kane Basin. A modelling study of Nares Strait projecting sea ice and hydrographic conditions from 1952 to 2080 CE predicted a decline in sea-ice cover and a fresher sea surface (Rasmussen et al., 2011). Our observations suggest that these modelled changes are already underway.

The presence of ice-bridges in Nares Strait plays a crucial role in maintaining the highly productive NOW Polynya, a climate sensitive ecosystem (Ribeiro et al., 2021), and satellite data indicate a potential decline in its productivity (Marchese et al., 2017). This raises the possibility that areas of open water supporting higher productivity may be shifting northward into Kane Basin. A long-term study covering periods where both ice bridges were lacking have shown that the configuration led to increased drift-ice export through Nares Strait and a subsequent decline in primary production (Georgiadis et al., 2020). This suggests that the recent increase in productivity observed in Kane Basin is likely associated with the selective presence of the northern ice bridge.

5 Conclusion

In this study, we analysed two marine sediment records spanning approximately 250 years from two locations within Kane Basin. We show significant spatial variability across the basin in terms of sediment delivery, primary productivity, and source of organic matter. We attribute the difference in primary production between the sites to several factors including hydrodynamic conditions, nutrient availability, oceanographic differences, and biological differences. Both records also reveal temporal changes, transitioning from cold sea-surface conditions with extensive sea ice during the Late LIA (peaking around 1900 CE), towards more open and stratified waters, accompanied by increased primary production from approximately 1950 CE to present. Despite these spatial differences, both records display similar temporal patterns, indicating cold sea-surface conditions and extensive sea ice coverage peaking around 1900 CE. These reconstructions align with the most severe

https://doi.org/10.5194/egusphere-2025-2641
Preprint. Discussion started: 8 July 2025

conditions characterizing the Late LIA, a period marked by widespread cooling. Around 1950 CE, we observed an increase in primary production and a shift towards a more autotrophic/mixotrophic dinoflagellate cyst assemblage. Additionally, we observe species indicative of stronger water column stratification and increased freshwater input. We attribute these changes to: (1) enhanced open-water conditions in Kane Basin and an increased freshwater flux through Nares Strait due to earlier ice
415 bridge break-up, and/or (2) increased meltwater discharge from the Greenland Ice Sheet.

Appendices

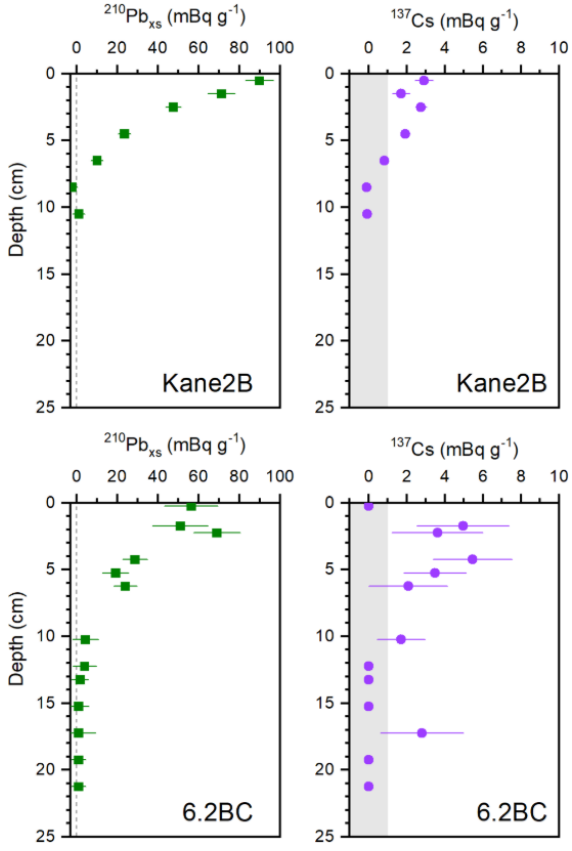

Figure A1: Profiles of 210Pbxs and of 137Cs with depth in cores Kane2B and 6.2BC. The grey area indicates 137Cs values that are not significant

https://doi.org/10.5194/egusphere-2025-2641
Preprint. Discussion started: 8 July 2025

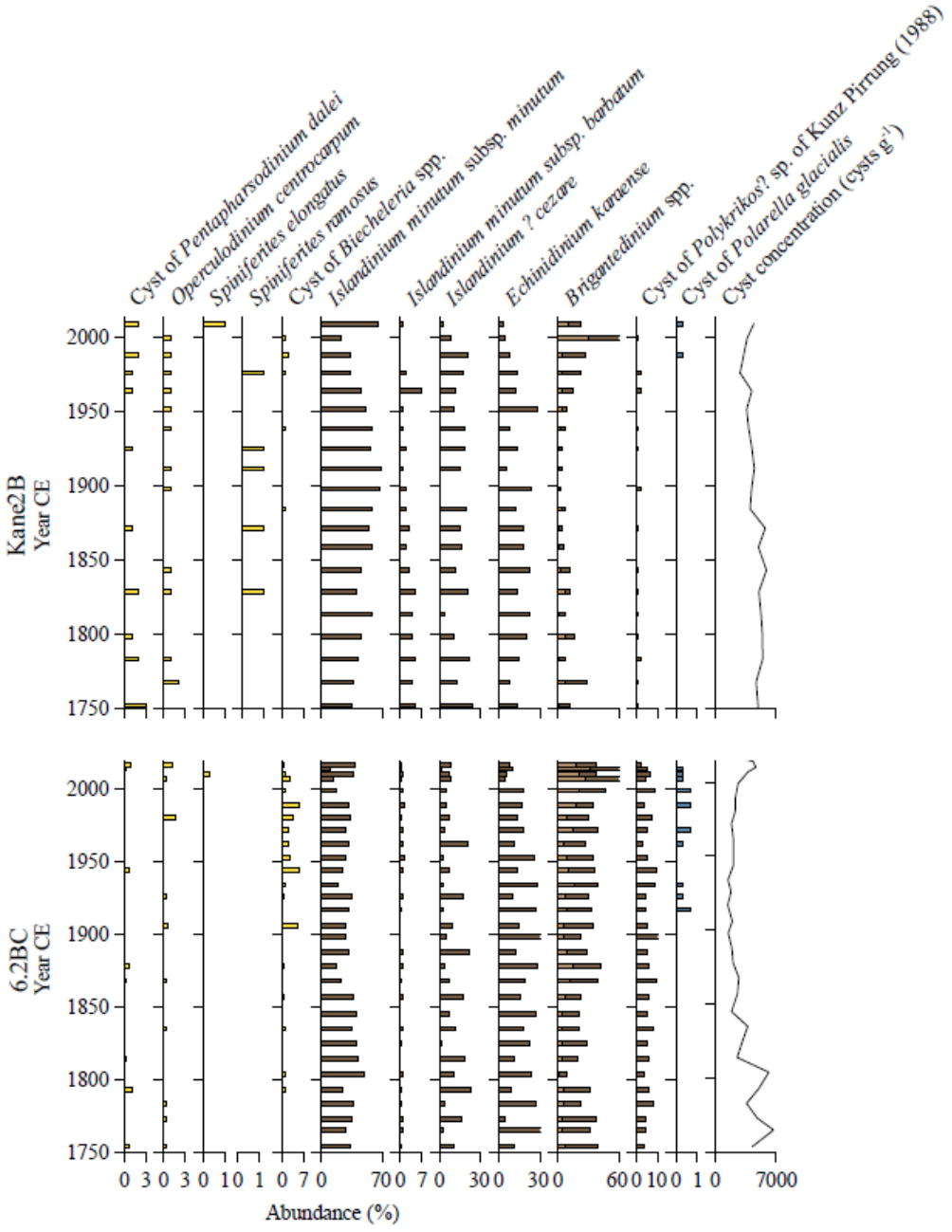

420 **Figure A2: Relative abundance (%) of dinoflagellate cyst taxa and cyst concentration (cysts g^{-1}) in record AMD14-Kane2B and AMD19-6.2BC. The autotrophic/mixotrophic species are shown in yellow and the heterotrophic dinoflagellate species in brown.**

https://doi.org/10.5194/egusphere-2025-2641
Preprint. Discussion started: 8 July 2025

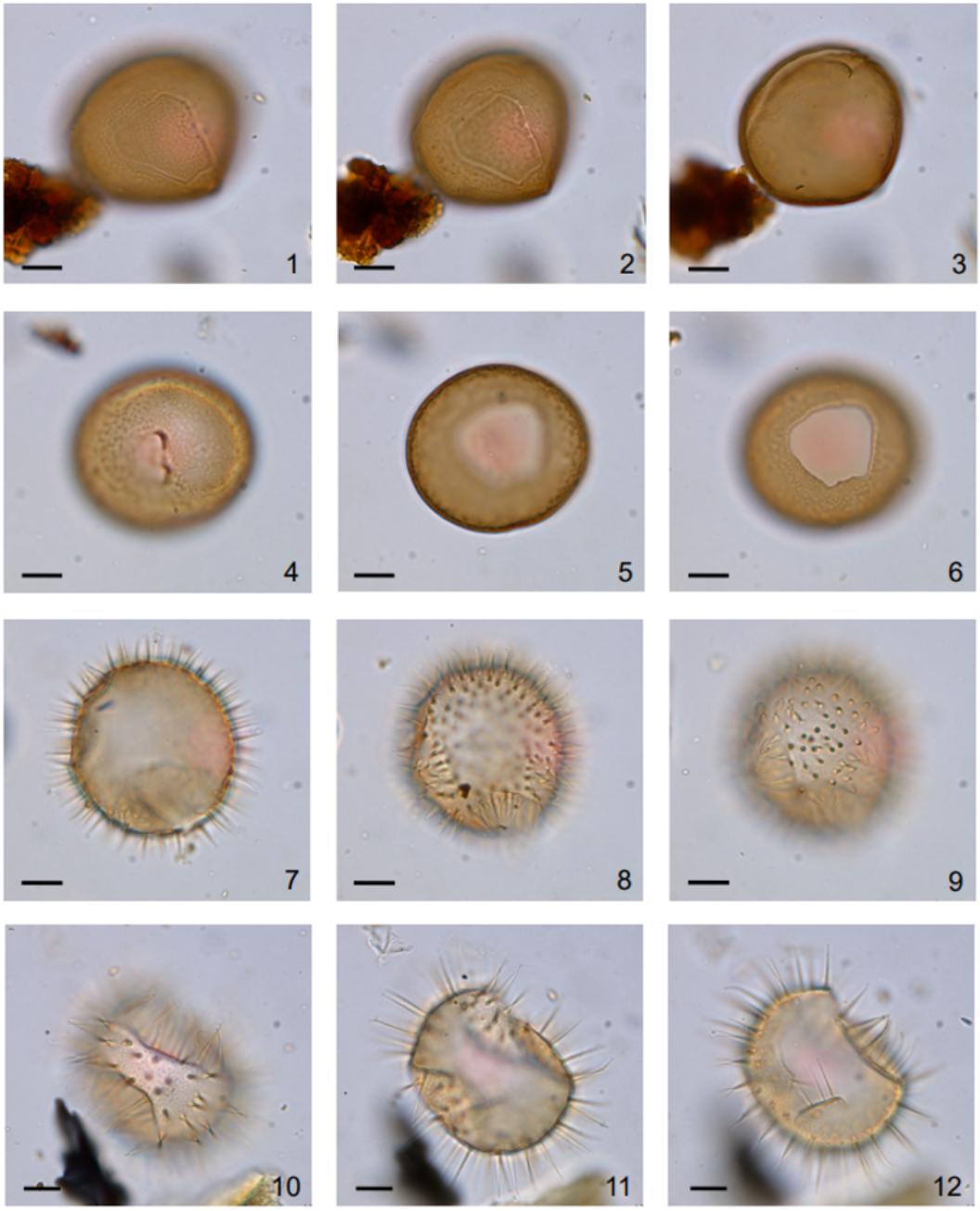

Figure A3: Dinoflagellate cyst plate from Kane2B. 1-6 high to low focus of *Brigantedinium simplex* with slightly granular surface. 1-3. Specimen with loosely attached operculum still in place. 7-9 high to low focus of *Islandinium minutum* subsp. *minutum*. 10-12 high to low focus of *Islandinium minutum* subsp. *barbatum*. Scale bar: 10 µm

https://doi.org/10.5194/egusphere-2025-2641
Preprint. Discussion started: 8 July 2025

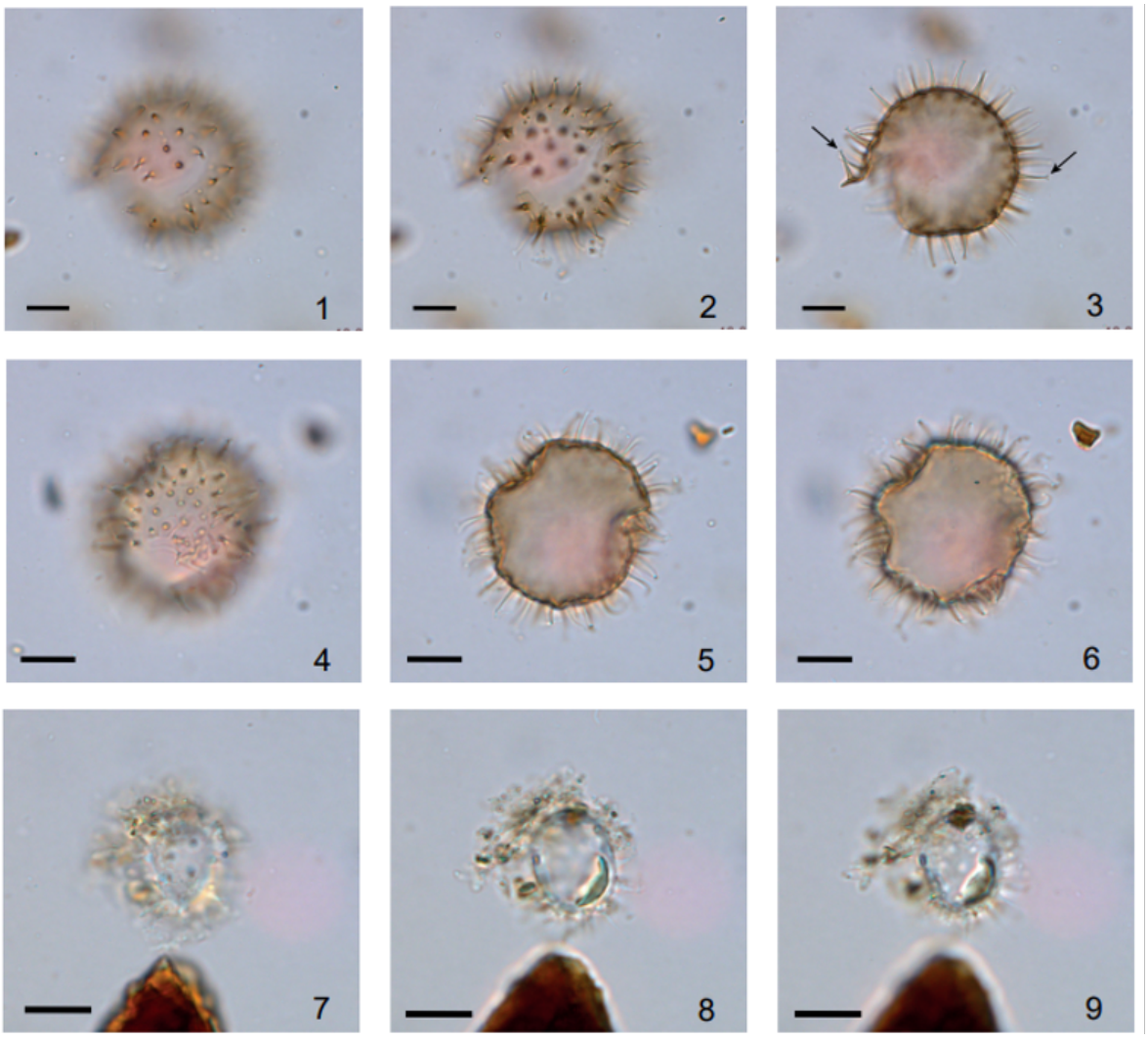

Figure A4: Dinoflagellate cyst plate from Kane2B. 1-3 high to low focus of *Echinidinium karaense*, arrows indicate the expanded and flared tip of some of the processes. 4-5 high to low focus of *Islandinium*? *cezare*. 7-9 high to low focus of *Polarella glacialis* cysts. Scale bar: 10 µm

430

https://doi.org/10.5194/egusphere-2025-2641
Preprint. Discussion started: 8 July 2025

Data availability

All the proxy data presented in the manuscript are available on the public data repository GEUS Dataverse (https://doi.org/10.22008/FK2/WT7P1E).

Author contribution

A.B.K. wrote the manuscript and generated all figures with input from all co-authors. S.R. conceived the study and provided extensive feedback and comments on the manuscript. M.-A.S. provided expert knowledge on biomarkers, G. L. helped generating parts of the figures. S.S and T. J. A helped generating the age-depth models. E. G., A. L., and J. G. contributed with expert knowledge on the area. A. A. B. and N. K. L. provided terrestrial context to the interpretations. All co-authors commented on the manuscript and approved its content.

Competing interests

The authors declare that they have no conflict of interest

Acknowledgements

We wish to thank the officers, crew members, scientific personnel, and the chief scientists of the ArcticNet 2014 and 2019 leg2 expeditions onboard the Canadian research icebreaker CCGS Amundsen for the collection of the sediment core material used in this project. MSc Mikkel Aagaard Frederiksen is greatly acknowledged for the laboratory work he conducted at GEUS.

Financial support

The fieldwork was conducted on board the Canadian research icebreaker CCGS Amundsen with the support of the Amundsen Science program funded by the Canada Foundation for Innovation (CFI) Major Science Initiatives (MSI) Fund and ArcticNet, a Network of Centres of Excellence in Canada

The project was funded by the Independent Research Fund Denmark (DFF-Sapere Aude grant no. 9064-00039B to Sofia Ribeiro).

https://doi.org/10.5194/egusphere-2025-2641
Preprint. Discussion started: 8 July 2025

References

Barão, L., Vandevenne, F., Clymans, W., Frings, P., Ragueneau, O., Meire, P., Conley, D. J., and Struyf, E.: Alkaline-extractable silicon from land to ocean: A challenge for biogenic silicon determination, Limnol Oceanogr Methods, 13, 329–344, https://doi.org/10.1002/lom3.10028, 2015.

Belt, S. T.: Source-specific biomarkers as proxies for Arctic and Antarctic sea ice, Org Geochem, 125, 277–298, https://doi.org/10.1016/j.orggeochem.2018.10.002, 2018.

Belt, S. T. and Müller, J.: The Arctic sea ice biomarker IP 25 : a review of current understanding , recommendations for future research and applications in palaeo sea ice reconstructions, Quat Sci Rev, 79, 9–25, https://doi.org/10.1016/j.quascirev.2012.12.001, 2013.

Belt, S. T., Massé, G., Rowland, S. J., Poulin, M., Michel, C., and Leblanc, B.: A novel chemical fossil of palaeo sea ice : IP25, ScienceDirect, 38, 16–27, https://doi.org/10.1016/j.orggeochem.2006.09.013, 2007.

Belt, S. T., Massé, G., Vare, L. L., Rowland, S. J., Poulin, M., Sicre, M.-A., Sampei, M., and Fortier, L.: Distinctive 13 C isotopic signature distinguishes a novel sea ice biomarker in Arctic sediments and sediment traps, Mar Chem, 112, 158–167, 2008.

Belt, S. T., Brown, T. A., Rodriguez, Al. N., Sanz, P. C., Tonkin, A., and Ingle, R.: Analytical Methods PAPER A reproducible method for the extraction , identification and quantification of the Arctic sea ice proxy IP 25 from marine sediments, The Royal Society of Chemistry, Analystical Methods, https://doi.org/10.1039/c2ay05728j, 2012.

Belt, S. T., Cabedo-Sanz, P., Smik, L., Navarro-Rodriguez, A., Berben, S. M. P., Knies, J., and Katrine Husum: Identification of paleo Arctic winter sea ice limits and the marginal ice zone: Optimised biomarker-based reconstructions of late Quaternary Arctic sea ice, Earth Planet Sci Lett, 431, 127–139, 2015.

Brown, T. A., Belt, S. T., Tatarek, A., and Mundy, C. J.: Source identification of the Arctic sea ice proxy IP 25, Nat Commun, 1–7, https://doi.org/10.1038/ncomms5197, 2014.

Burgers, T. M., Miller, L. A., Rysgaard, S., Mortensen, J., Else, B., Tremblay, J., and Papakyriakou, T.: Distinguishing Physical and Biological Controls on the Carbon Dynamics in a High-Arctic Outlet Strait, J Geophys Res Oceans, 128, https://doi.org/10.1029/2022JC019393, 2023.

https://doi.org/10.5194/egusphere-2025-2641
Preprint. Discussion started: 8 July 2025

Caron, M., Rochon, A., Montero-Serrano, J. C., and St-Onge, G.: Evolution of sea-surface conditions on the northwestern Greenland margin during the Holocene, J Quat Sci, 34, 569–580, https://doi.org/10.1002/jqs.3146, 2019.

Dahl-Jensen, D., Mosegaard, K., Gundestrup, N., Clow, G. D., Johnsen, S. J., Hansen, A. W., and Balling, N.: Past temperatures directly from the Greenland Ice Sheet, Science (1979), 282, 268–271, https://doi.org/10.1126/science.282.5387.268, 1998.

DeMaster, D. J.: Measuring biogenic silica in marine sediments and suspended matter, in: Marine Particles: Analysis and Characterization, Geophysical Monograph 63, American Geophysical Union, edited by: Hurd, D. C. and Spencer, D. W., Washington, D. C., 363–367, 1991.

Fernando, A., Freire, M., and Monteiro, M. C.: A Novel Approach for Inferring the Proportion of Terrestrial Organic Matter Input to Marine Sediments on the Basis of TOC : TN and δ 13 C org Signatures, Scientific Research, Open Journal of Marine Science, 3, 74–92, 2013.

Fol, M., Tremblay, B., Pfirman, S., Newton, R., Howell, S., and Lemieux, J. F.: Revisiting the Last Ice Area projections from a high-resolution Global Earth System Model, Commun Earth Environ, 6, 1–12, https://doi.org/10.1038/s43247-025-02034-5, 2025.

Georgiadis, E., Giraudeau, J., Martinez, P., Lajeunesse, P., St-Onge, G., Schmidt, S., and Massé, G.: Deglacial to postglacial history of Nares Strait, Northwest Greenland: A marine perspective from Kane Basin, Climate of the Past, 14, 1991–2010, https://doi.org/10.5194/cp-14-1991-2018, 2018.

Georgiadis, E., Giraudeau, J., Jennings, A., Limoges, A., Jackson, R., Ribeiro, S., and Massé, G.: Local and regional controls on Holocene sea ice dynamics and oceanography in Nares Strait, Northwest Greenland, Mar Geol, 422, 106115, https://doi.org/10.1016/j.margeo.2020.106115, 2020.

Goliber, S., Black, T., Catania, G., Lea, J. M., Olsen, H., Cheng, D., Bevan, S., Bjørk, A., Bunce, C., Brough, S., Carr, J. R., Cowton, T., Gardner, A., Fahrner, D., Hill, E., Joughin, I., Korsgaard, N. J., Luckman, A., Moon, T., Murray, T., Sole, A., Wood, M., and Zhang, E.: TermPicks: a century of Greenland glacier terminus data for use in scientific and machine learning applications, Cryosphere, 16, 3215–3233, https://doi.org/10.5194/tc-16-3215-2022, 2022.

Harðardóttir, S., Haile, J. S., Ray, J. L., Limoges, A., Van Nieuwenhove, N., Lalande, C., Grondin, P. L., Jackson, R., Skaar, K. S., Heikkilä, M., Berge, J., Lundholm, N., Massé, G., Rysgaard, S., Seidenkrantz, M. S., De Schepper, S., Lorenzen, E. D.,

https://doi.org/10.5194/egusphere-2025-2641
Preprint. Discussion started: 8 July 2025

Lovejoy, C., and Ribeiro, S.: Millennial-scale variations in Arctic sea ice are recorded in sedimentary ancient DNA of the microalga Polarella glacialis, Commun Earth Environ, 5, https://doi.org/10.1038/s43247-023-01179-5, 2024.

Hastie, T. J. and Tibshirani, R. J.: Generalized Additive Models, https://doi.org/10.2307/1269240, 1990.

Head, M. J., Harland, R., and Matthiessen, J.: Cold marine indicators of the late Quaternary: The new dinoflagellate cyst genus Islandinium and related morphotypes, J Quat Sci, 16, 621–636, https://doi.org/10.1002/jqs.657, 2001.

Heide-Jørgensen, M. P., Burt, L. M., Hansen, R. G., Nielsen, N. H., Rasmussen, M., Fossette, S., and Stern, H.: The significance of the north water polynya to arctic top predators, Ambio, 42, 596–610, https://doi.org/10.1007/s13280-012-0357-3, 2013.

Heikkilä, M., Pospelova, V., Hochheim, K. P., Kuzyk, Z. Z. A., Stern, G. A., Barber, D. G., and Macdonald, R. W.: Surface sediment dinoflagellate cysts from the Hudson Bay system and their relation to freshwater and nutrient cycling, Mar Micropaleontol, 106, 79–109, https://doi.org/10.1016/j.marmicro.2013.12.002, 2014.

Hillebrand, T. R., Hoffman, M. J., Perego, M., Price, S. F., and Howat, I. M.: The contribution of Humboldt Glacier, northern Greenland, to sea-level rise through 2100 constrained by recent observations of speedup and retreat, Cryosphere, 16, 4679–4700, https://doi.org/10.5194/tc-16-4679-2022, 2022.

Jakobsson, M., Mohammad, R., Karlsson, M., Salas-Romero, S., Vacek, F., Heinze, F., Bringensparr, C., Castro, C. F., Johnson, P., Kinney, J., Cardigos, S., Bogonko, M., Accettella, D., Amblas, D., An, L., Bohan, A., Brandt, A., Bünz, S., Canals, M., Casamor, J. L., Coakley, B., Cornish, N., Danielson, S., Demarte, M., Franco, D. Di, Dickson, M.-L., Dorschel, B., Dowdeswell, J. A., Dreutter, S., Fremand, A. C., Hall, J. K., Hally, B., Holland, D., Hong, J. K., Ivaldi, R., Knutz, P. C., Krawczyk, D. W., Kristofferson, Y., Lastras, G., Leck, C., Lucchi, R. G., Masetti, G., Morlighem, M., Muchowski, J., Nielsen, T., Noormets, R., Plaza-Faverola, A., Prescott, M. M., Purser, A., Rasmussen, T. L., Rebesco, M., Rignot, E., Rysgaard, S., Silyakova, A., Snoeijs-Leijonmalm, P., Sørensen, A., Straneo, F., Sutherland, D. A., Tate, A. J., Travaglini, P., Trenholm, N., Wijk, E. van, Wallace, L., Willis, J. K., Wood, M., Zimmermann, M., Zinglersen, K. B., Mayer, L., and 1Department: The International Bathymetric Chart of the Arctic Ocean (IBCAO), Sci Data, 11, 1–13, https://doi.org/10.1038/s41597-024-04278-w, 2024.

Jennings, A., Andrews, J., Reilly, B., Walczak, M., Jakobsson, M., Mix, A., Stoner, J., Nicholls, K. W., and Cheseby, M.: Modern foraminiferal assemblages in northern Nares Strait, Petermann Fjord, and beneath Petermann ice tongue, NW Greenland, Arct Antarct Alp Res, 52, 491–511, https://doi.org/10.1080/15230430.2020.1806986, 2020.

https://doi.org/10.5194/egusphere-2025-2641
Preprint. Discussion started: 8 July 2025

Jennings, A. E., Sheldon, C., Cronin, T. M., Francus, P., Stoner, J., and Andrews, J.: The Holocene History of Nares Strait, Transition from Glacial Bay to Arctic-Atlantic Troughflow, Oceanography, 24, 26–41, 2011.

Joli, N., Gosselin, M., Ardyna, M., Babin, M., Onda, D. F., Tremblay, J. É., and Lovejoy, C.: Need for focus on microbial species following ice melt and changing freshwater regimes in a Janus Arctic Gateway, Sci Rep, 8, 1–11, https://doi.org/10.1038/s41598-018-27705-6, 2018.

KDS: Satellite images from Sentinel 2 and SPOT 6/7 licensed under CC BY 4.0, Danish Agency for Climate Data, https://dataforsyningen.dk/data/4783, 2025.

Kim, Y. H., Min, S. K., Gillett, N. P., Notz, D., and Malinina, E.: Observationally-constrained projections of an ice-free Arctic even under a low emission scenario, Nat Commun, 14, 3–10, https://doi.org/10.1038/s41467-023-38511-8, 2023.

Kirillov, S., Babb, D. G., Komarov, A. S., Dmitrenko, I., Ehn, J. K., Worden, E., Candlish, L., Rysgaard, S., and Barber, D. G.: On the Physical Settings of Ice Bridge Formation in Nares Strait, J Geophys Res, 126, e2021, 0–19, https://doi.org/https://doi.org/10.1029/2021JC017331, 2021.

Kirillov, S., Dmitrenko, I., Babb, D. G., Ehn, J. K., Koldunov, N., Rysgaard, S., Jensen, D., and Barber, D. G.: The role of oceanic heat flux in reducing thermodynamic ice growth in Nares Strait and promoting earlier collapse of the ice bridge, Ocean Science, 18, 1535–1557, https://doi.org/10.5194/os-18-1535-2022, 2022.

Kjær, K. H., Bjørk, A. A., Kjeldsen, K. K., Hansen, E. S., Andresen, C. S., Siggaard-Andersen, M. L., Khan, S. A., Søndergaard, A. S., Colgan, W., Schomacker, A., Woodroffe, S., Funder, S., Rouillard, A., Jensen, J. F., and Larsen, N. K.: Glacier response to the Little Ice Age during the Neoglacial cooling in Greenland, Earth Sci Rev, 227, https://doi.org/10.1016/j.earscirev.2022.103984, 2022.

Klein, B., LeBlanc, B., Mei, Z. P., Beret, R., Michaud, J., Mundy, C. J., Von Quillfeldt, C. H., Garneau, M. È., Roy, S., Gratton, Y., Cochran, J. K., Bélanger, S., Larouche, P., Pakulski, J. D., Rivkin, R. B., and Legendre, L.: Phytoplankton biomass, production and potential export in the North Water, Deep Sea Res 2 Top Stud Oceanogr, 49, 4983–5002, https://doi.org/10.1016/S0967-0645(02)00174-1, 2002.

Koerner, K. A., Limoges, A., Van Nieuwenhove, N., Richerol, T., Massé, G., and Ribeiro, S.: Late Holocene sea-surface changes in the North Water polynya reveal freshening of northern Baffin Bay in the 21st century, Glob Planet Change, 206, https://doi.org/10.1016/j.gloplacha.2021.103642, 2021.

https://doi.org/10.5194/egusphere-2025-2641
Preprint. Discussion started: 8 July 2025

Koerner, K. A., Limoges, A., Pike-Connolly, E., Van Nieuwenhove, N., and Rochon, A.: Early impacts of Arctic amplification in the western North Water Polynya: A 400-year perspective, Mar Micropaleontol, 197–198, https://doi.org/10.1016/j.marmicro.2025.102470, 2025.

Kolling, H. M., Stein, R., Fahl, K., Sadatzki, H., de Vernal, A., and Xiao, X.: Biomarker Distributions in (Sub)-Arctic Surface Sediments and Their Potential for Sea Ice Reconstructions, Geochemistry, Geophysics, Geosystems, 21, https://doi.org/10.1029/2019GC008629, 2020.

Kumar, V., Tiwari, M., Nagoji, S., and Tripathi, S.: Evidence of Anomalously Low δ13C of Marine Organic Matter in an Arctic Fjord, Sci Rep, 6, 1–9, https://doi.org/10.1038/srep36192, 2016.

Lamb, A. L., Wilson, G. P., and Leng, M. J.: A review of coastal palaeoclimate and relative sea-level reconstructions using δ13C and C/N ratios in organic material, Earth Sci Rev, 75, 29–57, https://doi.org/10.1016/j.earscirev.2005.10.003, 2006.

Legendre, P. and Gallagher, ED.: Ecologically meaningful transformations for ordination of species data, Oecologia, 2, 271–280, https://doi.org/10.1007/s004420100716. Epub 2001 Oct 1. PMID: 28547606, 2001.

Marchese, C., Albouy, C., Tremblay, J. É., Dumont, D., D'Ortenzio, F., Vissault, S., and Bélanger, S.: Changes in phytoplankton bloom phenology over the North Water (NOW) polynya: a response to changing environmental conditions, Polar Biol, 40, 1721–1737, https://doi.org/10.1007/s00300-017-2095-2, 2017.

Meire, L., Mortensen, J., Meire, P., Juul-Pedersen, T., Sejr, M. K., Rysgaard, S., Nygaard, R., Huybrechts, P., and Meysman, F. J. R.: Marine-terminating glaciers sustain high productivity in Greenland fjords, Glob Chang Biol, 23, 5344–5357, https://doi.org/10.1111/gcb.13801, 2017.

Melling, H., Gratton, Y., and Ingram, G.: Ocean circulation within the North Water polynya of Baffin Bay, Atmosphere - Ocean, 39, 301–325, https://doi.org/10.1080/07055900.2001.9649683, 2001.

Meyers, P. A.: Preservation of Elemental and Isotopic Source Identification of Sedimentary Organic Matter, Chem Geol, Vol. 114, 289–302, https://doi.org/doi:10.1016/0009-2541(94)90059-0, 1994.

Miall, A. D.: Tertiary sedimentation and tectonics in the Judge Daly Basin, northeast Ellesmere Island, Arctic Canada. Energy, Mines, and Resources Canada., 1982.

https://doi.org/10.5194/egusphere-2025-2641
Preprint. Discussion started: 8 July 2025

Moore, G. W. K., Howell, S. E. L., Brady, M., Xu, X., and McNeil, K.: Anomalous collapses of Nares Strait ice arches leads to enhanced export of Arctic sea ice, Nat Commun, 12, 1–8, https://doi.org/10.1038/s41467-020-20314-w, 2021.

Mouginot, J., Rignot, E., Bjørk, A. A., van den Broeke, M., Millan, R., Morlighem, M., Noël, B., Scheuchl, B., and Wood, M.: Forty-six years of Greenland Ice Sheet mass balance from 1972 to 2018, Proc Natl Acad Sci U S A, 116, 9239–9244, https://doi.org/10.1073/pnas.1904242116, 2019.

Müller, J., Wagner, A., Fahl, K., Stein, R., Prange, M., and Lohmann, G.: Towards quantitative sea ice reconstructions in the northern North Atlantic: A combined biomarker and numerical modelling approach, Earth Planet Sci Lett, 306, 137–148, https://doi.org/10.1016/j.epsl.2011.04.011, 2011.

Mullin, J. B. and Riley, J. P.: The colorimetric determination of silicate with special reference to sea and natural waters, Anal Chim Acta, 12, 162–176, 1955.

Nutt, D. C.: The Drift of Ice Island WH-5, Arctic, 19, https://doi.org/10.14430/arctic3432, 1966.

Odate, T., Hirawake, T., Kudoh, S., Klein, B., LeBlanc, B., and Fukuchi, M.: Temporal and spatial patterns in the surface-water biomass of phytoplankton in the North Water, Deep Sea Res 2 Top Stud Oceanogr, 49, 4947–4958, https://doi.org/10.1016/S0967-0645(02)00172-8, 2002.

Oksanen, J., Simpson, G. L., Blanchet, F. G., Kindt, R., Legendre, P., Minchin, P. R., O'Hara, R. B., Solymos, P., Stevens, M. H. H., Szoecs, E., Wagner, H., Barbour, M., Bedward, M., Bolker, B., Borcard, D., Carvalho, G., Chirico, M., Caceres, M. De, Durand, S., Evangelista, H. B. A., FitzJohn, R., Friendly, M., Furneaux, B., Hannigan, G., Hill, M. O., Lahti, L., McGlinn, D., Ouellette, M.-H., Cunha, E. R., Smith, T., Stier, A., Braak, C. J. F. Ter, Weedon, J., and Borman, T.: _vegan: Community Ecology Package_. R package version 2.6-2, <https://CRAN.R-project.org/package=vegan>., 2022.

Quaijtaal, W., Donders, T. H., Persico, D., and Louwye, S.: Characterising the middle Miocene Mi-events in the Eastern North Atlantic realm: A first high-resolution marine palynological record from the Porcupine Basin, Palaeogeogr Palaeoclimatol Palaeoecol, 399, 140–159, https://doi.org/10.1016/j.palaeo.2014.02.017, 2014.

Rasmussen, T. A. S., Kliem, N., and Kaas, E.: The effect of climate change on the sea ice and hydrography in Nares Strait, Atmosphere - Ocean, 49, 245–258, https://doi.org/10.1080/07055900.2011.604404, 2011.

https://doi.org/10.5194/egusphere-2025-2641
Preprint. Discussion started: 8 July 2025

Ren, H., Shokr, M., Li, X., Zhang, Z., Hui, F., and Cheng, X.: Estimation of Sea Ice Production in the North Water Polynya Based on Ice Arch Duration in Winter During 2006–2019, J Geophys Res Oceans, 127, https://doi.org/10.1029/2022JC018764, 2022.

Ribeiro, S., Limoges, A., Massé, G., Johansen, K. L., Colgan, W., Weckström, K., Jackson, R., Georgiadis, E., Mikkelsen, N., Kuijpers, A., Olsen, J., Olsen, S. M., Nissen, M., Andersen, T. J., Strunk, A., Wetterich, S., Syväranta, J., Henderson, A. C. G., Mackay, H., Taipale, S., Jeppesen, E., Larsen, N. K., Crosta, X., Giraudeau, J., Wengrat, S., Nuttall, M., Grønnow, B., Mosbech, A., and Davidson, T. A.: Vulnerability of the North Water ecosystem to climate change, Nat Commun, 12, https://doi.org/10.1038/s41467-021-24742-0, 2021.

Rignot, E., An, L., Chauche, N., and Morlighem, M.: Retreat of Humboldt Gletscher , North Greenland , Driven by Undercutting From a Warmer Ocean Geophysical Research Letters, 0, 1–9, https://doi.org/10.1029/2020GL091342, 2019.

Schubert, C. J. and Calvert, S. E.: Nitrogen and carbon isotopic composition of marine and terrestrial organic matter in Arctic Ocean sediments: Implications for nutrient utilization and organic matter composition, Deep Sea Res 1 Oceanogr Res Pap, 48, 789–810, https://doi.org/10.1016/S0967-0637(00)00069-8, 2001.

Serreze, M. C. and Stroeve, J.: Arctic sea ice trends, variability and implications for seasonal ice forecasting, Philosophical Transactions of the Royal Society A: Mathematical, Physical and Engineering Sciences, 373, https://doi.org/10.1098/rsta.2014.0159, 2015.

Simpson, G. L.: Modelling palaeoecological time series using generalised additive models, Front Ecol Evol, 6, 1–21, https://doi.org/10.3389/fevo.2018.00149, 2018.

Stein, R. and Macdonald, R. W.: The Organic Carbon Cycle in the Arctic Ocean, 194 pp., https://doi.org/10.1007/978-3-642-18912-8, 2004.

Stoecker, D. K., Gustafson, D. E., Baier, C. T., and Black, M. M. D.: Primary production in the upper sea ice, Aquatic Microbial Ecology, 21, 275–287, https://doi.org/10.3354/ame021275, 2000.

Stroeve, J. C., Serreze, M. C., Holland, M. M., Kay, J. E., Malanik, J., and Barrett, A. P.: The Arctic's rapidly shrinking sea ice cover: A research synthesis, Clim Change, 110, 1005–1027, https://doi.org/10.1007/s10584-011-0101-1, 2012.

Team, R. C.: R: A language and environment for statistical computing. R Foundation for Statistical Computing, Vienna, Austria. URL https://www.R-project.org/., 2021.

https://doi.org/10.5194/egusphere-2025-2641
Preprint. Discussion started: 8 July 2025

de Vernal, A., Radi, T., Zaragosi, S., Van Nieuwenhove, N., Rochon, A., Allan, E., De Schepper, S., Eynaud, F., Head, M. J., Limoges, A., Londeix, L., Marret, F., Matthiessen, J., Penaud, A., Pospelova, V., Price, A., and Richerol, T.: Distribution of common modern dinoflagellate cyst taxa in surface sediments of the Northern Hemisphere in relation to environmental parameters: The new n=1968 database, Mar Micropaleontol, 159, 101796, https://doi.org/10.1016/j.marmicro.2019.101796, 2020.

Vincent, R. F.: A Study of the North Water Polynya Ice Arch using Four Decades of Satellite Data, Sci Rep, 9, 1–12, https://doi.org/10.1038/s41598-019-56780-6, 2019.

Williford, T., Amon, R. M. W., Kaiser, K., Benner, R., Stedmon, C., Bauch, D., Fitzsimmons, J. N., Gerringa, L. J. A., Newton, R., Hansell, D. A., Granskog, M. A., Jensen, L., Laglera, L. M., Pasqualini, A., Rabe, B., Reader, H., Rutgers van der Loeff, M., and Yan, G.: Spatial Complexity in Dissolved Organic Matter and Trace Elements Driven by Hydrography and Freshwater Input Across the Arctic Ocean During 2015 Arctic GEOTRACES Expeditions, J Geophys Res Oceans, 127, https://doi.org/10.1029/2022JC018917, 2022.

Wood, S. N.: Fast stable restricted maximum likelihood and marginal likelihood estimation of semiparametric generalized linear models, J R Stat Soc Series B Stat Methodol, 73, 3–36, https://doi.org/10.1111/j.1467-9868.2010.00749.x, 2011.